THE ASTROPHYSICAL JOURNAL, 342:834–854, 1989 July 15

MOLECULAR CLOUD CORES AND BIMODAL STAR FORMATION

SUSANA LIZANO AND FRANK H. SHU
Astronomy Department, University of California, Berkeley
Received 1988 May 23; accepted 1988 December 19

ABSTRACT

We review the phenomenon of bimodal star formation in the context of supercritical and subcritical states for molecular clouds that are supported against their self-gravitation by magnetic fields. For subcritical clouds, we formulate and solve the problem of the quasi-static condensation of a dense core from a more extended background by ambipolar diffusion. The computational space spans the tidal lobe, inside of which gravitational equipotential surfaces completely enclose the region of interest. In addition to magnetic support, we include the effects of thermal and "turbulent" pressures, with the latter receiving a semi-empirical treatment consistent with observational measurements of nonthermal line widths in molecular clouds. We find that subcritical regions can be conceptually divided in accordance to whether their masses are greater than an umbral mass (superumbral) or less (subumbral). Ambipolar diffusion operating in a subumbral region yields a stable final configuration in which the (mean) magnetic field asymptotically become uniform and straight, and the region, which has typically failed to become either dense enough or big enough to excite measurable ammonia emission, is balanced against gravitation by thermal and turbulent support. In contrast, the diffusion of ions and magnetic fields relative to a contracting sea of neutrals in a superumbral region will lead to the production of a centrally condensed core, that ultimately collapses from inside out (to form a star). For typical interstellar parameters, the sizes and densities of such cores correspond well with the observed properties of ammonia cores in the Taurus dark cloud, and the time scale to form these objects is also consistent with observations. Our calculations also support the view that the epoch of major flux loss occurs, not during the stage of (quasi-static) core formation, but during the much denser dynamic stage of protostar formation. Furthermore, we confirm that the mass scale of forming stars is set not by the interstellar medium but probably by processes (e.g., stellar winds) that occur in the stars themselves.

Subject headings: hydromagnetics — interstellar: molecules — stars: binaries — stars: formation

I. INTRODUCTION

a) *Bimodal Star Formation*

In a recent review (Shu, Adams, and Lizano 1987, hereafter SAL), we argued that in self-gravitating molecular clouds, supported primarily by magnetic fields, star formation proceeds bimodally (see also Mestel 1985).

1. Clouds (or clumps) with a mass $M_{\rm cl}$ less than a critical value $M_{\rm cr}$ are *subcritical* and cannot be induced to contract indefinitely by any amount of increased external pressure if the magnetic flux Φ is conserved. With field freezing, any compression of the cloud also increases the field in exact proportion for the magnetic forces to keep pace with the increased gravitational attraction. For a subcritical cloud, then, collapse will occur only by magnetic flux redistribution, which is driven, for a lightly ionized medium, by ambipolar diffusion (Mestel and Spitzer 1956; see also Mouschovias 1978). The frictional coupling is usually strong enough in the early stages to guarantee that the evolution occurs quasi-statically through a sequence of equilibrium states (Nakano 1979), wherein the neutral components gradually slip past the charged particles and the magnetic fields that provide the basic support. With a large initial ratio of magnetic to thermal pressure (so that the Jeans mass $M_{\rm J} \ll M_{\rm cl}$), many small dense cores would slowly condense from the common envelope of an extended region, an outcome descriptive of the Taurus molecular cloud (e.g., Myers and Benson 1983). This mode constitutes an ongoing background process for the formation of individual or binary stars in nearly every self-gravitating molecular cloud. Empirically, by the time the cores acquire densities high enough ($>3 \times 10^4$ cm^{-3} within a radius of $\sim$0.05 pc) to excite measurable ammonia emission, about half of them have collapsed to form low-mass stars (Beichman *et al.* 1986). Since the ages of deeply embedded infrared sources of modest luminosities (low-mass protostars) are estimated to lie between 10^5 and 10^6 yr (Stahler, Shu, and Taam 1980; Adams and Shu 1986; Adams, Lada, and Shu 1987), this observation suggests that the lifetimes of molecular cloud cores, once they have reached central concentrations characteristic of the NH_3 observations, cannot much exceed 10^5–10^6 yr. This estimate provides an important constraint on proposed mechanisms for the origin of the small dense cores (see also Myers *et al.* 1987).

2. Clouds (or clumps) with a mass $M_{\rm cl}$ greater than a critical mass $M_{\rm cr}$ are *supercritical* and can collapse dynamically as a whole, overwhelming the internal magnetic support, even if the fields remain frozen in the fluid (e.g., Scott and Black 1980). Shu (1987) suggested that the production of supercritical regions from an ensemble of subcritical clouds could naturally arise by the agglomeration of clumps of gas and dust that have been gathered together in a large complex (Giant Molecular Clouds, or GMCs). Such a picture may provide a basis for understanding the triggering of OB stars behind galactic shocks and within the nuclear regions of starburst galaxies. This mode of star formation requires basically a high surface density of molecular material. Upon the cloud's flattening along the direction of the mean field, fragments of a size comparable to the cloud's thickness can themselves collapse as supercritical regions (Mestel 1965), yielding either a compact group of OB stars (e.g., Keto, Ho, and Haschick 1987; Welch *et al.* 1987), or a bound cluster if a high efficiency of star forma-

tion is not disrupted by the formation of too many luminous stars (e.g., Lada and Wilking 1984). The signature of a supercritical region would be coherent dynamical collapse involving large amounts (say, $\sim 10^2$–$10^5\ M_\odot$) of molecular gas. Other effects may be an elevation of the temperature of the gas relative to the dust by the effects of ion-neutral frictional heating (e.g., Wilking and Lada 1983; Lizano and Shu 1987) and a more disordered overall field configuration (Strom 1988).

b) *Magnetic Critical Mass*

The numerical value of the critical mass $M_{\rm cr}$ can be ascertained by virial theorem arguments (Strittmatter 1966), or more accurately by detailed model calculations (Mouschovias 1976). When magnetic fields alone provide support against gravity, the results can be expressed generically by the simple formula,

$$M_{\rm cr} = cG^{-1/2}\Phi\ , \tag{1}$$

where G is the universal gravitational constant and c is a dimensionless coefficient having a value $\sim$0.1–0.2, depending on the adopted mass-to-flux distribution and boundary conditions (Tomisaka, Ikeuchi, and Nakamura 1988, hereafter TIN). For example, an extrapolation of the Figure 1 by Mouschovias and Spitzer (1976) to zero $(p_{\rm T}/p_m)^{1/3}$ yields $c = 0.13$ for the case in which a uniform magnetic field initially threads a homogeneous spherical cloud. In § VI, we shall generalize the definition of the critical mass to take into account "turbulence" as a mechanism of cloud support in addition to magnetic fields (and thermal pressure).

c) *Goals of this Study*

In this paper, we make detailed three-dimensional models (with axial symmetry) of the mechanism of core formation by ambipolar diffusion from a larger subcritical region. Simple one-dimensional slab models (Shu 1983; Scott 1984; Nakano 1985) yield adequate estimates for the overall time required to condense a core from a rarefied envelope; however, the saturation of the gravitational field associated with a slab of constant surface density gives misleading results for the total amount of flux redistribution during the later stages and for the conditions required to initiate ultimate gravitational collapse (compare, e.g., the views of Mouschovias, Paleologou, and Fiedler 1985 with those of SAL and Nakano 1988). The extensive set of three-dimensional axisymmetric calculations of Nakano (1979, 1982, 1983) are more trustworthy in this regard; unfortunately, they focus on a parameter regime corresponding to magnetic field strengths and gas densities that are generally too large to be applicable to the ammonia cores observed as the sites of low-mass star formation (e.g., Myers and Goodman 1988; Goodman *et al.* 1988).

The above comments motivate the present set of calculations, wherein we study the quasi-static evolution of an axisymmetric periodic chain of self-gravitating regions ("tidal lobes") as ambipolar diffusion lowers the amount of magnetic and "turbulent" support in the dense cores. We choose boundary conditions that mimic the situation of many dense cores embedded within the common envelope of a much larger cloud (or clump). Our formulation of the condensation process allows us only to follow the quasi-static stages; an *a posteriori* check allows us to estimate the point at which the core evolution would suffer a transition to dynamical collapse.

In § II we derive the governing set of equations, subject to the quasi-static and axisymmetric approximations (and to appropriate boundary and initial conditions, which are discussed in § IV). In § III we outline the method of numerical solution and tests of the resultant computer code. In § V we discuss the results of the evolutionary calculations, emphasizing time scales, masses, and typical sizes of modeled cores that can be compared with observations. For a fixed mass, we find that the level of turbulent support determines whether a dense core forms or not. This allows us in § VI to generalize the concept of a critical mass to account for the contributions of turbulence and thermal pressure for helping magnetic fields to support a cloud. We then introduce the concept of an *umbral* mass that specifies the mass needed to overcome the remaining means of support after ambipolar diffusion has tried to straighten out the magnetic field lines in a subcritical cloud. Finally, in § VII we draw the implications of this work for the problem of star formation and comment on possible future work in this area.

II. GOVERNING EQUATIONS

a) *Formulation of the Basic Problem*

Consider the situation of a large number of cloud cores, spaced at an average distance $2L$ apart from one another inside a much more massive clump of molecular gas. We isolate our attention on a single core, whose center lies at the origin of a cylindrical coordinate system (ϖ, φ, z), embedded within a region of radius and half-height equal to L. If we assume local axial symmetry with the presence of only a *poloidal* magnetic field $\boldsymbol{B}$, then $\boldsymbol{B}$ is derivable from a vector potential $\boldsymbol{A}$ that has only a φ component:

$$\boldsymbol{A} = \frac{\Phi(\varpi, z, t)}{2\pi\varpi}\,\boldsymbol{e}_\varphi\ , \tag{2}$$

where $\Phi(\varpi, z, t) = \int_S \boldsymbol{B}\cdot\boldsymbol{e}_z\, 2\pi\varpi\, d\varpi$ is the magnetic flux at time t threading a circular area S of radius ϖ located at height z. The magnetic field is given by

$$\boldsymbol{B} = \nabla\times\boldsymbol{A} = \frac{1}{2\pi\varpi}\left(-\frac{\partial\Phi}{\partial z}\,\boldsymbol{e}_\varpi + \frac{\partial\Phi}{\partial\varpi}\,\boldsymbol{e}_z\right). \tag{3}$$

We assume that the cloud cores are well separated, i.e., that the spacing $2L$ is appreciably larger than the typical radii of identifiable NH_3 cores, so that the structure of the molecular cloud clump can be taken to be smooth in between cores. (The polarization observations of Vrba, Strom, and Strom 1976 and Moneti *et al.* 1984 show that the magnetic fields of dark clouds are well ordered on a large scale.) This allows us to impose the requirement that the magnetic field has uniform strength B_0 and is directed along the z-direction on our cell walls. If, in addition, we impose periodic boundary conditions in the z-direction (see § III), we find that the magnetic flux Φ, the neutral gas density ρ_n, and the gravitational potential V may all be taken to be even functions of z.

By definition, the magnetic field $\boldsymbol{B}$ is tangent to flux tubes, i.e., $\boldsymbol{B}\cdot\nabla\Phi = 0$, and the numerical value of the enclosed flux Φ can be used to label field lines. The nonlinear diffusion equation (16) for the magnetic field in SAL (hereafter abbreviated as eq. [SAL.16]) can now be written

$$\frac{D\Phi}{Dt} = -\boldsymbol{v}_d\cdot\nabla\Phi\ , \tag{4}$$

where $D/Dt = \partial/\partial t + \boldsymbol{u}_n\cdot\nabla$ is the substantial (or Lagrangian) time derivative following the motion $\boldsymbol{u}_n$ of the neutrals, and

where the drift velocity of ions relative to neutrals (see eq. [SAL.14]) is

$$\boldsymbol{v}_d = \frac{-1}{16\pi^3\gamma\rho_n\rho_i\varpi^2}\left(\frac{\partial^2\Phi}{\partial\varpi^2}+\frac{\partial^2\Phi}{\partial z^2}-\frac{1}{\varpi}\frac{\partial\Phi}{\partial\varpi}\right)\nabla\Phi\,. \tag{5}$$

In the above, γ equals the frictional drag coefficient (see eq. [SAL.13]) and has been estimated by Draine, Roberge, and Dalgarno (1983) to have a numerical value equal to 3.5×10^{13} cm^3 g^{-1} s^{-1} for the conditions of interest here (see also Mouschovias and Paleologou 1981).

For the ion mass density ρ_i, we adopt the steady state calculations of Elmegreen (1979) that result in the approximate relationship,

$$\rho_i = \mathscr{C}\rho_n^{1/2}\,, \tag{6}$$

where $\mathscr{C}$ is a weak function of gas temperature and is proportional to the square root of the metal depletion. For average metal depletions (i.e., a factor of 0.1), a cosmic-ray ionization rate equal to $\zeta = 1 \times 10^{-17}$ s^{-1}, and gas temperatures 10–30 K, Elmegreen obtains results which correspond to $\mathscr{C} = 3 \times 10^{-16}$ cm$^{-3/2}$ g$^{1/2}$. In this work we will ignore the effect of negatively charged grains because Nakano (1984, 1985) found that including their presence increased the ambipolar diffusion time scale by much less than a factor of 2 at the neutral gas densities $\ll 10^7$ cm^{-3} that characterize typical ammonia cores. Henceforth, we shall use equation (6) to eliminate ρ_i wherever it appears and simply denote ρ_n as ρ.

To account heuristically for the mechanical support provided by interstellar "turbulence" (see Larson 1981), we suppose a total gas pressure P,

$$P = P_{\rm th} + P_{\rm turb}\,, \tag{7}$$

given by the sum of the thermal pressure,

$$P_{\rm th} = a^2\rho\,, \tag{8}$$

where $a^2 \equiv kT/m$ is the square of the isothermal sound speed, and an isotropic "turbulent" contribution,

$$P_{\rm turb} = \mathscr{K}\ln(\rho/\rho_0)\,, \tag{9}$$

where $\mathscr{K}$ has a constant value and ρ_0 is some convenient reference density. We shall generally choose ρ_0 so that it has values representative of the common molecular envelope; however, any arbitrary constant could be added to $P_{\rm turb}$ without affecting the details of the forces exerted in the interior. The motivation for the functional form adopted in equation (9) is the empirical power-law correlation $\Delta v \propto \rho^{-1/2}$ found by various studies for the nonthermal part of molecular line widths (Solomon and Sanders 1985; Dame *et al.* 1986; Myers 1987; Scoville *et al.* 1987; see McKee 1989 for a review). If we interpret this correlation as an effective transport speed,

$$v_{\rm turb} = (dP_{\rm turb}/d\rho)^{1/2} = (\mathscr{K}/\rho)^{1/2}\,, \tag{10}$$

we obtain the identification, equation (9). The best fit for the data assembled by Myers and Goodman (1988) suggests that $\mathscr{K} = 1.2 \times 10^{-11}$ dyne cm^{-2}; the "cold" and "hot" GMCs surveyed by Solomon *et al.* (1987) have values of $\mathscr{K}$ which are 1.5 and 6 times larger. Although equation (9) has an empirical basis, the ultimate reason for choosing this particular functional form is for the mathematical convenience of having a barotropic equation of state when a^2 and $\mathscr{K}$ are taken to be constants. Notice that the support provided by turbulence drops relative to thermal pressure at high densities.

In our opinion (see SAL), the turbulence seen in molecular clouds, which is highly supersonic in the envelopes, reflects the presence of many nonlinear MHD waves (Arons and Max 1975); thus, for the problem of the dissipation of these waves, we consider it important to demonstrate that consistent cloud models can be constructed in which the fluctuating fluid motions are sub-Alfvénic. This demonstration is carried out in § V. We also need to enquire on the effects that Alfvénic turbulence would have for the problem of ambipolar diffusion. Zweibel (1988) has investigated the latter problem and concludes that, for the conditions likely to hold in molecular clouds, the effect is small. Consequently, in our further deliberations, we shall ignore all transport characteristics associated with the turbulence, apart from its ability to impart momentum changes through an effective scalar pressure (see the discussion in § VII); and henceforth, when we speak of ambipolar diffusion, we shall implicitly refer only to the slippage of the *mean magnetic field*, not to the fluctuating components.

With the above preamble, we are ready to consider the axisymmetric matter distribution of our equilibrium clouds. Within each diffusion time step, we assume quasi-static equilibrium (see Nakano 1979). The solution of this subproblem, with the mass-to-flux distribution fixed by its value at the previous instant, is greatly facilitated by adopting the method introduced by Mouschovias (1976) for computing magnetostatic equilibria (see also TIN). The existence of a barotropic equation of state follows us to introduce an enthalpy function h,

$$h = \int\frac{dP}{\rho} + V\,. \tag{11}$$

Under the assumption that forces are balanced, equation (SAL.18) can now be written as

$$\rho\nabla h = \boldsymbol{f}_d\,,$$

where $\boldsymbol{f}_d = \gamma\rho_n\rho_i\boldsymbol{v}_d$ is the drag force between ions and neutral (see eq. [SAL.13]), and is equal to the Lorentz force $(1/4\pi)(\nabla\times\boldsymbol{B})\times\boldsymbol{B}$. These considerations demonstrate that $\boldsymbol{B}\cdot\nabla h = 0$; therefore, force balance along field lines is satisfied if h is a function of Φ and t alone, i.e., $h = h(\Phi, t)$. In what follows we shall suppress explicit display of the variable t when dealing with the quasi-static aspects of the problem. Force balance across field lines then requires

$$\rho\frac{dh}{d\Phi} = \frac{-1}{16\pi^3\varpi^2}\left(\frac{\partial^2\Phi}{\partial\varpi^2}+\frac{\partial^2\Phi}{\partial z^2}-\frac{1}{\varpi}\frac{\partial\Phi}{\partial\varpi}\right), \tag{12}$$

where we have substituted equation (5) for the drift velocity in the drag force, $\boldsymbol{f}_d$.

b) *Nondimensionalization*

It pays to introduce dimensionless variables. Henceforth, we describe the density ρ in units of the fiducial value ρ_0 (used to obtain a convenient, rather than a fundamental, set of units; see footnote 1), the gravitational potential V and the enthalpy function h in units of the square of the sound speed a^2, and magnetic fields in units of a "background value" (in the molecular cloud envelope) B_0. These are the primary scalings; secondary scalings are lengths in units of l_0 (for example, the dimensionless spacing between consecutive cores is $2l \equiv 2L/l_0$),

magnetic flux in units of Φ_0, and time in units of t_0, where the latter quantities are defined by

$$l_0 = \frac{a}{(4\pi G\rho_0)^{1/2}} \equiv \frac{a^2\mathscr{R}}{G^{1/2}B_0}, \tag{13}$$

$$\Phi_0 = \frac{a^2 B_0}{2G\rho_0} \equiv \frac{2\pi a^4\mathscr{R}^2}{GB_0}, \tag{14}$$

$$t_0 = \left[\frac{\gamma\mathscr{C}}{(4\pi G)^{1/2}}\right]\left[\frac{1}{(4\pi G\rho_0)^{1/2}}\right] \equiv \left[\frac{\gamma\mathscr{C}}{(4\pi G)^{1/2}}\right]\frac{a\mathscr{R}}{G^{1/2}B_0}. \tag{15}$$

In the above, $\mathscr{R}$ is the ratio

$$\mathscr{R} = v_{A0}/a \tag{16}$$

of the reference Alfvén speed, $v_{A0} \equiv B_0/(4\pi\rho_0)^{1/2}$, to the sound speed a; and the combination $\gamma\mathscr{C}/(4\pi G)^{1/2}$ is the dimensionless large parameter of the problem whose square justifies a quasi-static treatment of the momentum equation (see Shu 1983). We further introduce a unit of mass,

$$m_0 = 4\pi\rho_0 l_0^3 \equiv \frac{a^4\mathscr{R}}{G^{3/2}B_0}. \tag{17}$$

The coefficient in the above expression has been chosen to express the mass-to-flux distribution (see eq. [21]) in a convenient form.

If we use the same symbols for the dimensionless variables as their dimensional counterparts, the equation (12) for force balance across field lines becomes the following partial differential equation (PDE) for Φ:

$$\mathscr{R}^2\left(\frac{\partial^2\Phi}{\partial\varpi^2} + \frac{\partial^2\Phi}{\partial z^2} - \frac{1}{\varpi}\frac{\partial\Phi}{\partial\varpi}\right) = -\varpi^2\rho\frac{dh}{d\Phi}. \tag{18}$$

The enthalpy function, defined by equation (11), can be integrated to give

$$h = K\left(1 - \frac{1}{\rho}\right) + \ln\rho + V, \tag{19}$$

where

$$K = \frac{\mathscr{K}}{a^2\rho_0} \tag{20}$$

is a dimensionless constant that yields $(v_{turb}/a)^2$ at the reference density ρ_0. The function $h(\Phi)$ is to be found so that a nondimensional integration for the mass-to-flux distribution yields the desired $dM/d\Phi$:

$$\frac{dM}{d\Phi} = \int dz\,\frac{\varpi(\Phi, z)\rho(\Phi, z)}{(\partial\Phi/\partial\varpi)_z}, \tag{21}$$

where the integration is performed from the equator to the tidal lobe along lines of constant Φ in the meridional plane.

Poisson's equation in nondimensional form becomes

$$\frac{\partial^2 V}{\partial\varpi^2} + \frac{\partial^2 V}{\partial z^2} + \frac{1}{\varpi}\frac{\partial V}{\partial\varpi} = \rho. \tag{22}$$

Time dependence enters in the problem through the dimensionless version of the diffusion equation (4):

$$\frac{D\Phi}{Dt} = \frac{(\mathscr{R}|\nabla\Phi|)^2}{\rho^{3/2}\varpi^2}\left(\frac{\partial^2\Phi}{\partial\varpi^2} + \frac{\partial^2\Phi}{\partial z^2} - \frac{1}{\varpi}\frac{\partial\Phi}{\partial\varpi}\right). \tag{23}$$

Notice that the diffusion stops if the field lines ever become straight and uniform, $\Phi = \varpi^2/2$.

We see from the above that two dimensionless parameters $\mathscr{R}$ and K enter in our formulation of the nondimensional equations. One more dimensionless parameter, $l \equiv L/l_0$, enters from the periodic boundary conditions; a fourth, the degree of central concentration of the "reference state"—or equivalently the total mass M_{tot} within the "tidal lobe" measured in units of m_0—enters in the procedure that we use to define the mass-to-flux distribution in the initial state (see § IV). Because ρ_0 is purely fiducial (there is no *characteristic* density in a molecular cloud, especially not near cores), only the three dimensionless combinations, l^2K, $l\mathscr{R}$, and M_{tot}/l are truly independent.[1] A space of solutions that varies in two spatial dimensions and time and that is controlled by three independent parameters is almost impossible to explore thoroughly. To date, except for a few isolated cases, we have only followed the complete evolutions of a sequence of models in which the $\mathscr{R}$, $2l$, and M_{tot} are held fixed ($R = 7.2$, $2l = 4.0$, and $M_{tot} = 7.0$), and the turbulence parameter K is allowed to vary within reasonable limits. The rationale for singling out this sequence is discussed below and in § IV.

"Standard" Choice of Parameters

Our interpretation of the extensive observational literature concerning dark clouds like Taurus suggests a "standard" set of dimensional parameters: a kinetic temperature $T = 10$ K and mean molecular mass $m = 2.3m_H$ (resulting in an isothermal sound speed $a = 0.19$ km s^{-1}); a reference (envelope) density $\rho_0/m = 1 \times 10^3$ cm^{-3}; and a background magnetic field of $B_0 = 30$ μG. These choices yield $\mathscr{R} = 7.2$ (i.e., and Alfvén speed equal to 1.4 km s^{-1} at a density of 10^3 cm^{-3}), and we also have

$$l_0 = 0.11 \text{ pc}, \quad \Phi_0 = 2.5\ \mu G\ \text{pc}^2, \quad m_0 = 0.96\ M_\odot.$$

A choice of $2l = 4.0$ therefore represents an average separation between cores of $\sim$0.44 pc, which is probably somewhat on the low side for the Taurus molecular cloud. Our adoption of the value $2l = 4.0$ represents a compromise between realism and sufficient numerical resolution to model the interior structure of a condensing ammonia core (whose diameter characteristically spans only 0.1 pc). As an additional aside, we note that the coincidence between the above numerical value for m_0 and typical observed masses of ammonia cores (the mass inside a density contour = 3×10^4 cm^{-3}) is purely accidental.

If we now further adopt the values of γ and $\mathscr{C}$, cited in the previous subsection, we have an intrinsic diffusion time scale (associated with contraction from the envelope)

$$t_0 = 6 \times 10^6 \text{ yr}$$

[1] A fundamental choice of units could be based on a, L, and G, from which we could arrange $\mathscr{K}$, B_0, and $\mathscr{M}_{tot}$ (as we temporarily denote the dimensional total mass inside the tidal lobe in order to avoid confusion) into the three dimensionless combinations: $4\pi GL^2\mathscr{K}/a^4 = l^2K$, $G^{1/2}LB_0/a^2 = l\mathscr{R}$, and $G\mathscr{M}_{tot}/La^2 = M_{tot}/l$. Nondimensionalization of the equations could then be based on the scalings: $\rho_L \equiv a^2/4\pi GL^2$, $m_L \equiv a^2L/G$, $B_L \equiv a^2/G^{1/2}L$, $\Phi_L \equiv 2\pi a^2L/G^{1/2}$, $t_L \equiv [\gamma\mathscr{C}(4\pi G)^{1/2}](L/a)$. Because only the derivatives of P_{turb} and h enter in the calculations, the fiducial density ρ_0 appears nowhere in this formulation, either in the governing equations or in the boundary conditions (see eqs. [31] and [32]). Hence, apart from numerical convenience in comparisons with observations, the only rationale for introducing ρ_0 is conceptual—so that we can think in terms of independently varying the core spacing ($2l$), the level of turbulence (K), the envelope magnetic field ($\mathscr{R}$), and the total mass inside the tidal lobe (M_{tot}).

that is nearly an order of magnitude longer than the dynamical time of the material inside the tidal lobe. As we shall see, however, the evolutionary time for a condensed ammonia core (the central region of the tidal lobe) can become much shorter than t_0.

The adoption of $\mathscr{K} = 1.2 \times 10^{-11}$ dyne cm^{-2} gives $K = 8.7$. This value holds roughly in the envelopes of "cold" clouds as well as their cores. For example, in the ammonia cores of Taurus (densities $> 3 \times 10^4$ cm^{-3}), Myers and Benson (1983) obtain a mean turbulent contribution to the line width that is typically only 60% of sonic (corresponding to $K = 11$). Moreover, if one eliminates the cores that have already formed stars (Fuller and Myers 1987), the turbulent contribution drops to only 45% of sonic (corresponding to $K = 6$). Our strategy, then, will be to compute a number of cases spanning such values for K.

Even though we will discuss results bearing in mind the standard dimensional set of parameters above, models with given $\mathscr{R}$ and l can, of course, be scaled to other physical situations by the judicious use of equations (13), (14), (15), and (17). For example, with a reference density $\rho_0/m = 500$ cm^{-3}, a background magnetic field $B_0 = 21$ μG (to correspond to $\mathscr{R} = 7.2$), and the same temperature $T = 10$ K, the scalings are $l_0 = 0.16$ pc, $\Phi_0 = 3.6$ μG pc^2, $t_0 = 8.5 \times 10^6$ yr, and the mass unit is $m_0 = 1.4$ $M_\odot$. With $2l = 4.0$, these choices yield bigger physical separations between cores and contain (for a given nondimensional $M_{\rm tot}$) 40% more mass and flux within a given cell than the "standard case." The dimensionless critical density needed to excite NH_3 emission is now $\rho = 60$ (instead of $\rho = 30$), and so the dimensionless calculation has few grid points inside the central core region, and therefore less numerical resolution. Moreover, K needs to be increased by a factor of 2 if we are to have the same *observed* ratio for turbulent to thermal speeds in the ammonia cores.

III. METHOD OF SOLUTION

To compute the evolution of the region, the equations (18), (22), and (23) are put into a difference form (spatially centered to give second-order accuracy) and solved together with the transcendental equation (19) on an Eulerian grid with equal spacing Δ. As explained earlier, we follow Nakano (1979) in calculating the quasi-static evolution via a set of equilibrium states. In this scheme the time development enters only through the diffusion equation (23).

a) *Diffusion Step*

The principal computational trick that we adopt is to give an operator-splitting interpretation for the substantial derivative D/Dt in equation (23). In the first part of the split, D/Dt is interpreted as $\partial/\partial t$, i.e., we diffuse the magnetic flux relative to a *fixed* distribution of neutrals. The explicit advance in time of equation (23) is performed with small time steps $\sim(\Delta/l\mathscr{R})^2$ to avoid numerical instabilities. This typically requires tens of thousands of small time steps to be taken to complete one evolutionary calculation. After a number of small time steps (typically a hundred), whose aggregate we refer to as a "diffusion step," we update the resulting configuration for force balance. We achieve a new force balance by solving the equations of mechanical equilibrium, (18) and (22), subject to the constraint of *field freezing*, with the new mass-to-flux distribution obtained from the first part of the operator-splitting calculation. Thus, in the second part of the split, we effectively treat D/Dt as $\boldsymbol{u}_n \cdot \nabla$, except that the scheme requires no explicit calculation for the neutral velocity $\boldsymbol{u}_n$, although it is recoverable after the fact (see Appendix). This step of finding the equilibrium configuration given a fixed mass-to-flux distribution, equation (21), is well described by Mouchovias (1976); we modify his technique only in the details by which we carry out the iterative relaxations for the numerical solution of the governing elliptic equations (see below).

b) *Algorithm to Achieve Force Balance*

1. For a guessed density ρ, we obtain the gravitational potential V by solving Poisson's equation (22). We choose a relaxation method (see below) rather than a direct solver because the evolution proceeds through many diffusion steps, and it would be wasteful not to use the information available from the solution at the previous configuration as the first guess to achieve by iteration a current solution (which involves only a slightly changed state).

2. Given the potential V, a new specific enthalpy $h(\Phi)$ and a new density ρ are found such that $dM/d\Phi$ is correct. This is done by solving the specific enthalpy equation (19), as a transcendental equation for the density ρ given a guessed functional form for $h(\Phi)$ and the given gravitational potential V. The guessed $h(\Phi)$ is corrected using Newton's method, until the correct mass-to-flux distribution (eq. [21]) is obtained.

3. With this new density ρ and enthalpy h, force balance across field lines, equation (18), is solved as an elliptic PDE for the magnetic flux Φ, again using a relaxation technique (see below).

These three steps are repeated until the gravitational potential V, the density ρ, and the magnetic flux Φ are self-consistent. We are then ready to take another diffusion step (see previous subsection).

c) *Elliptic Equations and Relaxation Method*

Given appropriate boundary and initial conditions (see § IV), we outline below the relaxation method by which we solve the elliptic PDEs (18) and (22) for the magnetic flux Φ and the gravitational potential V. (More details are given in Lizano 1988.) Let Ψ represent either Φ or V.

1. We solve the centered difference equation algebraically for Ψ on all interior grid points (i, j) in terms of their nearest neighbors $(i \pm 1, j)$ and $(i, j \pm 1)$. We denote this operation schematically by the equation,

$$\Psi = \mathscr{D}\Psi , \tag{24}$$

where $\mathscr{D}$ is a discrete averaging operator that may contain inhomogeneous terms (i.e., terms that involve $dh/d\Phi$ or ρ). Using the values of the previous iterate for the nearest neighbors on the right-hand side of equation (24), we call the formal solution obtained for the left-hand side, the intermediate iterate Ψ^*.

2. A new iterate Ψ is constructed by taking a fraction $(1 - \xi)$ of the intermediate Ψ^* and a fraction ξ of the previous iterate, resulting in the equation,

$$\Psi = \Psi^* - \xi\,\delta\Psi , \tag{25}$$

where $\delta\Psi$ represents the difference between the intermediate iterate and the previous iterate. The quantity ξ is the relaxation parameter, and it is commonly chosen to be 0.5, a value that works reasonably well, at least empirically, under a wide variety of circumstances. The technique to be described below uses a variable ξ that considerably speeds up the rate of convergence (often by an order of magnitude in benchmark tests).

Steps 1 and 2 are repeated to find a solution that satisfies

$$\mathscr{L}\Psi \equiv \Psi - \mathscr{D}\Psi = 0 \tag{26}$$

on all nonboundary grid points. After any finite number of iterations, $\mathscr{L}\Psi$ will, in general, not be zero; we now outline our method for choosing the relaxation parameter ξ so as to maximize the rate at which $\mathscr{L}\Psi$ approaches zero in a global sense.

We begin by defining a global error function,

$$\epsilon^2(\xi) \equiv \sum_{ij} (\mathscr{L}\Psi)^2 = \sum_{ij} (\mathscr{L}\Psi^* - \xi \mathscr{L}\,\delta\Psi)^2 , \tag{27}$$

where the sum is over all interior grid points and where we have made use of the fact that $\mathscr{L}$ is a linear operator when ρ and h are regarded as known. When expanded out algebraically, the global error is a quadratic function of ξ:

$$\epsilon^2(\xi) = p\xi^2 - 2q\xi + r , \tag{28}$$

where

$$p \equiv \sum_{ij} (\mathscr{L}\,\delta\Psi)^2 , \tag{29a}$$

$$q \equiv \sum_{ij} (\mathscr{L}\Psi^*)(\mathscr{L}\,\delta\Psi) , \tag{29b}$$

$$r \equiv \sum_{ij} (\mathscr{L}\Psi^*)^2 . \tag{29c}$$

Therefore, the positive-definite error $\epsilon^2(\xi)$ will be minimized for *each* iteration step when ξ is chosen to be

$$\xi = q/p . \tag{30}$$

The relaxation parameter ξ determined this way can have any value, positive or negative, and, unlike other arbitrary choices, is guaranteed (almost) to produce convergence. (The worst that one could do is to choose the previous iterate as the next guess, i.e., choose $\xi = 1$; thus, the minimized error decreases monotonically as one iterates. Values of ξ between 0 and 1 correspond to underrelaxation; less than zero, to overrelaxation; greater than 1, to going "backward"—i.e., previous iterates were "better" than current ones.) In practice, this technique greatly accelerates convergence at the initial stages, but the improvement in the solution at the final stages (when the solution is almost "correct") is slow. The calculation of ϵ^2 gives us an explicit estimate of the global error involved in the solution of the finite-difference representation of our governing PDEs; we usually continue to iterate until the quantity $|\mathscr{L}\Psi/\Psi|$ is less than 10^{-6} at each grid point.

d) Tests of Numerical Code

Differences in the adopted boundary conditions and the lack of tabular results in the published papers prevented a comparison of the developed numerical code with the results of Nakano (1979, 1982, 1983) and the equilibria of Mouschovias (1976) and TIN. Instead, we conducted two other tests. First, we considered the toy problem of an infinite cylinder supported against gravity in the ϖ direction by magnetic pressure, gas pressure, and rotation at a uniform angular rate Ω about the z-axis. For the infinite cylinder, solution of the governing one-dimensional equations can easily be found by the Henyey technique (linearization about a previous iterate followed by inversion of tridiagonal matrices). The two-dimensional (axisymmetric three-dimensional) code presented in this paper does not include rotation, but the case of uniform rotation can easily be introduced by replacing the gravitational potential V with an effective potential $V_{\rm eff} = V - \Omega^2\varpi^2/2$. On carrying out the test, we found agreement between the two methods of solution to better than 1% for grids containing as few as 20 points (in both ϖ and z-dimensions in the two-dimensional code).

Cylindrical clouds have limited density contrasts in comparison to configurations contracting axisymmetrically in three-dimensions. Our second test thus concerned the capability of the two-dimensional code to resolve a large dynamic range. To do this, we solved the ordinary differential equation (see, e.g., Chandrasekhar 1939) governing the structure of a self-gravitating sphere that has the barotropic equation of state, (7), considered in this paper. We then compared this accurate density distribution with that obtained by the two-dimensional code when we included a uniform magnetic field (one that exerts no forces) and the same boundary conditions. As long as we used grids with 40 or more points in each dimension, our two-dimensional solutions gave density distributions that agreed everywhere to better than 5% with the exact results even for density contrasts between the center and the surface that reached 1000. For larger density contrasts, our ability to resolve the center diminishes rapidly. Fortunately, the evolutionary calculations in § V show that molecular cloud cores with such high degrees of central concentration are likely to be in a state of dynamical collapse, so our capacity for following the true quasi-static stages is not seriously impaired by the use of relatively coarse gridding (40 points in each dimension).

IV. BOUNDARY CONDITIONS, REFERENCE STATES, AND INITIAL STATES

a) Boundary Conditions

To mimic the physical situation of the existence of many dense regions (cores) in a much larger molecular cloud, we consider an infinite periodic chain of identical cells strung out along the z-axis. Needless to say, our posed scenario is highly idealized; in fact, the global structure so envisaged is unstable, a condition which may be resolved by real cores possessing motions relative to one another. Such motions are ignored by our assumption that core centers maintain a constant spacing equal to the cell dimension, $2L$. Nevertheless, there does exist observational evidence that suggests the relative motions of cloud cores in the Taurus cloud to be small (Benson 1983; Fuller 1988), perhaps less than even the isothermal sound speed, $a = 0.19$ km s^{-1}. Thus, the idealization that the centers of the individual cells have no relative motion with respect to each other probably represents a reasonable first step in trying to model the substructure of as complicated an object as a real molecular cloud.

Consistent with the above approximation, the gravitational potential associated with the chain of condensations will define (nearly fixed) *tidal lobes*, inside of which the equipotentials will form closed surfaces that encompass the condensing cores completely, and outside of which the equipotential surfaces will connect to the entire chain (i.e., open to the common envelope). To compute the location of the tidal lobe exactly through the actual implementation of periodic boundary conditions would require us to know the distribution of matter in the common envelope. Since we do not know how to give a realistic description for the state of the common envelope, we choose to formulate our problem so as to apply all boundary conditions on the tidal lobe of a given cell (centered on the origin). To locate the tidal lobe, we assume that no mass is exchanged between the condensing cloud core and the common envelope. This fixes the mass inside the tidal lobe for all times to be equal to that present initially.

To the extent that the actual mass distribution inside a cell can be approximated by an "equivalent" spherical one so that higher multipole contributions are negligible, we may compute the location of the tidal lobe by considering a chain of point masses. We can then easily demonstrate that the locus of the tidal lobe is given by

$$\psi(\varpi, z) \equiv \sum_{j=-\infty}^{\infty} \left\{ \frac{1}{[\varpi^2 + (2jl - z)^2]^{1/2}} - \frac{1}{|2j - 1|l} \right\} = 0 . \quad (31)$$

For $\varpi = 0$, the solution passes through X-shaped cusps (saddle points of the potential) at $z = \pm l$. (Notice all lengths in eq. [31] scale with l, i.e., the solution written in normalized variables $\varpi' \equiv \varpi/l$ and $z' \equiv z/l$ is universal [see footnote 1].) On the locus $\psi(\varpi, z) = 0$, the (Dirichlet) boundary conditions (in nondimensional form) for equations (18) and (22) become

$$V = V_{\rm chain} \quad \text{and} \quad \Phi = \varpi^2/2 \text{ at the tidal lobe,} \quad (32a)$$

where $V_{\rm chain}$ is the potential (an arbitrary constant) due to the chain of gravitating cells.

The concept of an infinite chain of identical cells gives only one possible realization for the tidal lobe. As formulated above, an alternative procedure would have been to focus on a single self-gravitating region from the start, and to define the tidal forces on it implicitly by specifying V = constant on an arbitarily shaped locus, $\psi(\varpi, z) = 0$, with X-points at $(\varpi, z) = (0, \pm l)$. In any case, with the specific form (fixed for all time) given by equation (31), the axial and reflection symmetries discussed in § II*a* make it unnecessary to solve the equations inside the entire tidal lobe. One can consider just the upper right quadrant of the meridional plane by including the additional (Neumann and Dirichlet) boundary conditions for V and Φ:

$$\frac{\partial V}{\partial \varpi} = 0 \quad \text{and} \quad \text{at } \Phi = 0 \quad \text{at } \varpi = 0 , \quad (32b)$$

$$\frac{\partial V}{\partial z} = 0 \quad \text{and} \quad \frac{\partial \Phi}{\partial z} = 0 \quad \text{at } z = 0 , \quad (32c)$$

that correspond to no gravitational force normal to the ϖ- and z-axes, no source of magnetic fields on the z-axis, and no component of B_ϖ on the ϖ-axis.

Notice that the imposition of a fixed outer location (tidal lobe) for a given mass of gas ($M_{\rm tot}$), together with equations (32a)–(32c), makes incompatible any further specification of outer boundary conditions; in particular, we do not (indeed, cannot) require that the density just outside the tidal lobe equals ρ_0 (i.e., that the pressure just outside the tidal lobe have some given value). Thus, in what follows below, we shall find that ρ in the initial state varies as a function of position along the tidal lobe, and that, furthermore, as a function of time, it tends to drop slightly at each such position when the interior contracts because of ambipolar diffusion. Implicit in the fixing of $M_{\rm tot}$ for the mass within the tidal lobe is the assumption that the common envelope behaves in whatever manner necessary to satisfy the resulting consequences imposed by our adopted boundary conditions. (Recall that boundary conditions lie external to the region governed by the differential equations of the problem and represent merely the *prejudice* of the scientist concerning what the rest of the world is like outside of the system under discussion.) We consider the resultant behavior (slight lowering of the boundary pressures as a function of time) reasonable for the present case of an infinite chain of identically contracting molecular cloud cores. For the opposite extreme of an *isolated* core, the tendency of a large reservoir of matter in the envelope to barostat the "surface pressure" of the cell at its initial value (by allowing matter to slide along field lines across the tidal lobe) should remove the restriction that $M_{\rm tot}$ is a constant (or that $dM/d\Phi$ is fixed between diffusion steps). This equally interesting alternative deserves a study of its own and will not be discussed further in the present treatment. We merely note that the total drop of "surface pressure" of the cell before the core undergoes a transition to dynamical collapse is not large in the cases calculated in the present paper, so that the inclusion of a slow accretion of material across the tidal lobe would probably not have affected the results very much except to hasten the earlier stages of the core-formation process.

In any case, if the tidal lobe is located sufficiently far from the central regions occupied by the condensing core, then the important part of the solution should not be sensitive to details of the outer boundary conditions. In the case of the gravitational potential, this expectation is borne out by *a posteriori* checks of the various contributions to the total gravitational energy associated with a given cell. We find that even in our initial states (described below), less than 10% of the total gravitational energy comes from the contribution of the external potential due to matter outside the tidal lobe. The self-gravitational isolation of the core increases as ambipolar diffusion enhances its central concentration; consequently, many of our conclusions concerning the evolution of molecular cloud cores should hold independently of the detailed implementation of outer boundary conditions.

b) Reference States

With the boundary conditions described above for Poisson's equation, we may compute by our relaxation technique a self-consistent *reference* state that includes the elongation imposed by the tidal forces. (An adequate zeroth-order guess is a spherical distribution supported against self-gravity by the gas pressure in eq. [7], as discussed for the second of the test problems in § III*d*.) Once the self-consistent (nonspherical) mass distribution has been found, we thread the gas with a straight and uniform magnetic field of unit dimensionless strength (dimensional strength B_0). This defines the dimensionless mass-to-flux distribution for our reference state. A field configuration which has $\Phi = \varpi^2/2$ everywhere, and not just at the tidal lobe, exerts, of course, no magnetic force anywhere, so our reference state is still in exact magnetostatic equilibrium.

The upper left diagram of Figure 1 shows the equipotential contours of a reference state, with the location of the tidal lobe appearing as a dark curve. The corresponding isodensity contours are shown in the upper right diagram of Figure 1. The jagged heavy line represents the nearest grid point to the tidal lobe. To simplify bookkeeping in the code, outer boundary conditions are imposed on these grid points by interpolation from the actual tidal lobe. The logarithmic density profiles of the reference state, along the ϖ- and z-directions, are displayed in the lower left diagram of Figure 1. Notice that a high value for K (30) keeps the density contrast low—a factor of only 1.75 from the center to the tidal lobe—so that the mass-to-flux distribution would be similar (but not identical), in a non-dimensional sense, to the completely uniform reference states of Mouchovias (1976) and TIN (called by them as "initial" states). This (somewhat arbitrary) prejudice limits the range over which the total mass $M_{\rm tot}$ can differ from the "surface" density times the volume of the tidal lobe. For the reference state described here, $M_{\rm tot} = 7.0$ (in units of m_0). The fractional

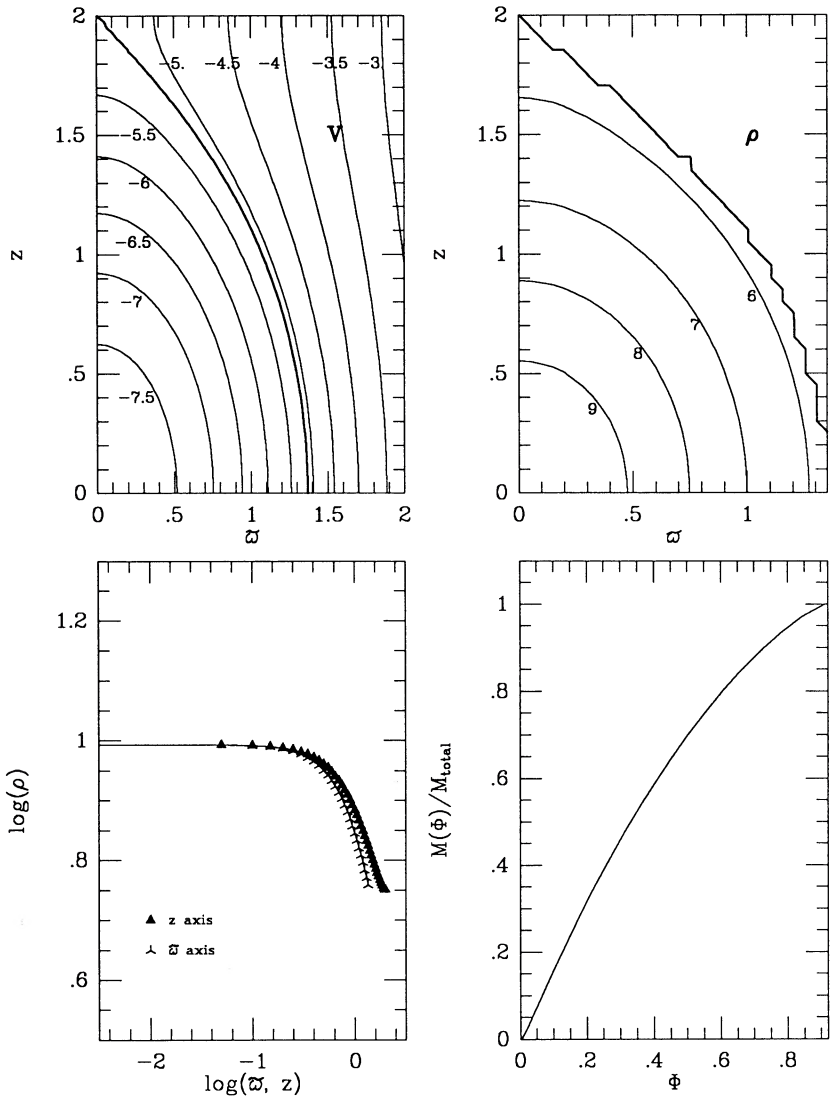

FIG. 1.—The reference state. (*a*) Equipotential contours, labeled by their values, $V = -7.5$, -7.0, -6.5, -6.0, -5.5, -5.0, -4.5, -4.0, -3.5, and -3.0, are shown in the upper left diagram for one quadrant of the meridiidional plane. The tidal lobe, characterized by $V_{chain} = -5.13$, is drawn as a dark curve, and separates closed and open equipotential surfaces. (*b*) Isodensity contours are shown in the upper right diagram, with labels marking $\rho = 9$, 8, 7, and 6. The jagged heavy curve marks the nearest grid point to the tidal lobe. In the absence of magnetic forces, isodensity contours lie on equipotential contours, a fact obscured in these diagrams by the different scales adopted for the horizontal axes. (c) Logarithmic density profiles, along the ϖ- and z-axes, are shown in the lower left diagram. Notice the relatively small degree of central concentration of the reference state. (*d*) The mass $M(\Phi)$ enclosed inside the flux tube Φ as a fraction of the total M_{tot} inside the tidal lobe is shown in the lower right diagram. The assumed spatial distribution for the magnetic field is uniform and straight, i.e., $\Phi = \varpi^2/2$.

mass $M(\Phi)/M_{tot}$ contained within a given flux tube Φ is shown in the lower right diagram of Figure 1. Since the total flux Φ_{tot} is 0.91 (in units of Φ_0), the total mass-to-flux ratio in the cell $M_{tot}/\Phi_{tot} = 7.7$, and has been adjusted, by our intention to focus on a self-gravitating region, to exceed the critical mass-to-flux ratio defined by equation (1) (5.9 if $c = 0.13$). Although our reference state is supercritical by this definition, it is, in fact, stabilized against dynamical collapse by the nonmagnetic means of support (principally "turbulence"). This comment alerts us to the necessity of a better definition for the "critical" mass in circumstances when forces other than magnetic fields contribute appreciably to cloud support (see § VI).

c) *Initial States*

The equilibrium of the reference state in Figure 1 is maintained by an artificially high level of turbulence (K equal to 30). To obtain realistic *initial states*, we decrease the value of K (to 14 or lower), while performing iterations to maintain force balance and field freezing. In this fashion, we gradually replace turbulent support by increasing amounts of magnetic support. This procedure automatically introduces curvature of the field lines, for the same mass-to-flux distribution as the reference state, and leads to a flattening of the inner portions of the cloud. Figure 2 shows the resulting equilibria for the values of the turbulent parameter $K = 12$, 10, 6, and 2. Notice that the densities at the tidal lobe (no longer a single value for a given K) become smaller than the reference state. The effect arises by gas settling along field lines and compressing the central regions to dimensionless densities of $\rho_c = 13$, 16, 23, and 72, respectively. The last equilibrium state, $K = 2$, is highly condensed. It already looks like an ammonia core and contains a mass of 0.94 (in units of m_0) within the isodensity contour of 30.

If ambipolar diffusion were allowed to proceed (see § V), the core would increase its degree of central concentration extremely quickly ($< 10^5$ yr), and go into a state of dynamical collapse.

We do not ask how the prior evolution of a molecular cloud clump (turbulent decay, or gas motions along field lines, or ambipolar diffusion in the envelope over the natural time of $\sim t_0$) might have led to the production of the magnetostatic equilibria seen in Figure 2, but arbitrarily reset the clock at $t = 0$ for each of them. With these *initial states*, then, we follow their *future* evolution to develop (or not to develop) condensed cores through the subsequent process of ambipolar diffusion of the ions and magnetic field. The results of our evolutionary calculations are discussed in the next section.

V. RESULTS OF QUASI-STATIC EVOLUTION BY AMBIPOLAR DIFFUSION

The evolution of a large number of initial states was computed by varying the turbulent parameter K, in a sequence where the Alfvén parameter $\mathscr{R}$, the dimensionless spacing $2l$, and the dimensionless total mass $M_{\rm tot}$ within the tidal lobe were held fixed at 7.2, 4.0, and 7.0, respectively. We discuss here only three representative cases: $K = 6$, $K = 10$, and $K = 12$. In particular, we shall show that when the turbulent parameter is

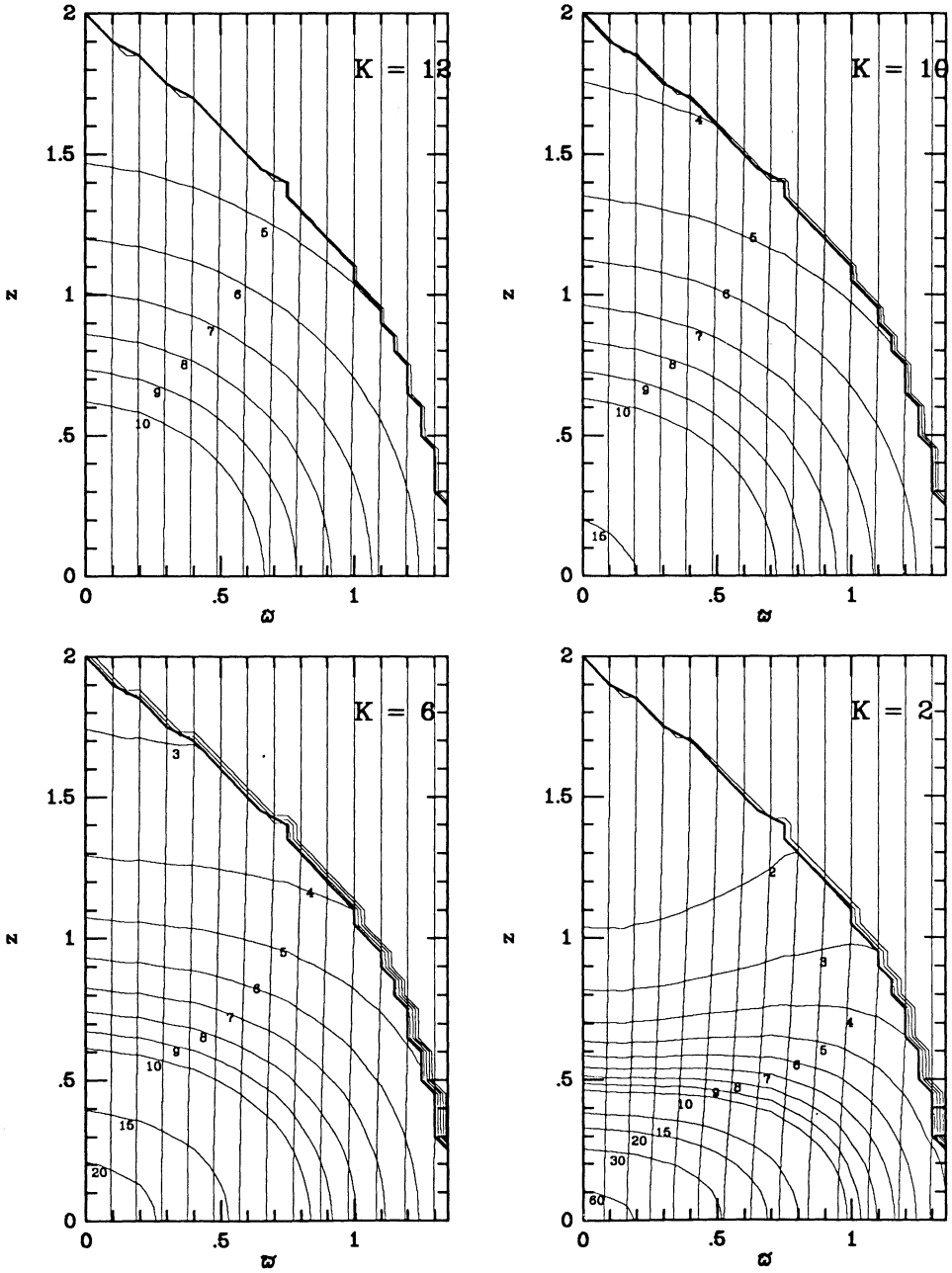

FIG. 2.—Initial states, equilibria for the values of the turbulent parameter $K = 12$,10, 6, and 2, with isodensity contours as marked. The central densities are $\rho_c = 13$, 16, 23, and 72, respectively. The piling up of the contours at the position of the nearest grid point to the tidal lobe is an artifact of the plotting routine. The equilibrium state corresponding to $K = 2$ is already fairly condensed and would be observable as an ammonia core.

sufficiently small, ambipolar diffusion of the magnetic field in molecular clouds can quasi-statically produce, within the requisite time scale, centrally condensed pockets of gas and dust having the observed properties of ammonia cores. Moreover, since the contraction is very nonhomologous, with the center evolving quickly compared to the outer regions, the developing core will eventually collapse from *inside-out* to form stars in the qualitative manner originally envisaged by Shu (1977).

To check the quasistatic approximation, we estimate the velocity of the neutrals by the method explained in the Appendix. We do not carry the computations beyond the time when these velocities become sonic along field lines (see below). To show the evolution of the magnetic flux tubes in time, we will always plot the set of magnetic flux tubes that cross the tidal lobe (where $\Phi = \varpi^2/2$) at the axial positions $\varpi = 0.1$–1.3 in steps of 0.1. For ease of visualization, the field lines beyond this point in the common envelope are plotted as being uniform in strength and vertical in direction, which introduces a very slight kink at the tidal lobe for the displayed models. This kink has no physical significance (e.g., in terms of current sheets) since no equations for the cloud or field structure were solved outside of the tidal lobe.

a) Evolution with Turbulent Parameter K = 6

The case $K = 6$ corresponds to a turbulent speed that is 45% of the isothermal sound speed at the density $\rho = 30$. Figure 3 shows the isodensity contours and magnetic flux tubes for this case at the time $t = 0.21$ (*solid lines*). The dashed lines indicate the location of the flux tubes at time $t = 0$. (To compare the density contours at $t = 0$, see Fig. 2.) Although the magnetic flux has diffused outward relative to the matter distribution by ambipolar diffusion, it has been dragged in, relative to an Eulerian grid, by the gravitational concentration of the neutrals. Therefore, the field strength B increases even though ambipolar diffusion is occurring (see below).

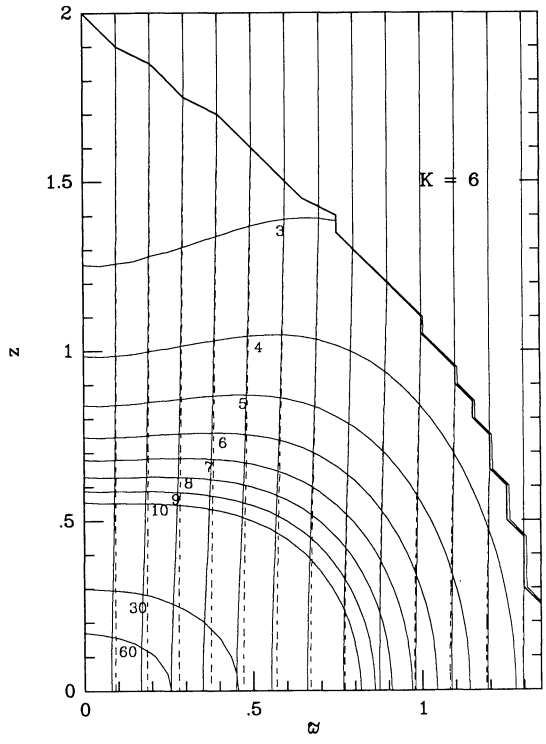

FIG. 3.—The superposition of isodensity contours and magnetic flux tubes for the case with $K = 6$ at the time $t = 0.21$ (*solid lines*). The dashed lines give the magnetic flux tubes at $t = 0$. Compare the density contours here with those at $t = 0$ as shown in Fig. 2.

From $t = 0$ to $t = 0.21$, the central density ρ_c has increased from an initial value 23 to a value 97, well in excess of the critical density 30 needed to excite ammonia emission (if we adopt the "standard set" of dimensional parameters mentioned in § II). At the time $t = 0.21$, the mass inside the density contour $\rho = 30$ is 1.0 (in units of m_0).

For $m_0 = 0.96\ M_\odot$, the mass contained within $\rho = 30$ is comparable to typical values measured for Taurus ammonia cores and to the inferred masses of the sunlike stars that they form. However, our calculations here explicitly demonstrate that the rough equality between the latter two masses is a pure coincidence; nothing special exists about the isodensity contour $\rho = 30$ that would distinguish it *mechanically* from $\rho = 10$ (or 100, or 1). If the material ($1.0m_0$) inside $\rho = 30$ were to fall into a star, without the interference of a protostellar outflow, nothing would prevent the entire mass $M_{\rm tot}$ inside the tidal lobe ($7.0m_0$) from following. Nor would the infall process stop there, because after this tidal lobe has emptied, material would be transferred over from neighboring tidal lobes (if gravitational collapse is not perfectly synchronized in all cells), as well as fall in from the common envelope. In other words, *no consideration of the mechanical properties of molecular clouds leads to a natural identification of stellar mass scales; stellar masses are likely to be determined by additional processes that occur inside the stars themselves* (see the review of SAL).

Returning to the discussion of our cloud model, we note that the radial extent of the $\rho = 30$ contour also agrees well (assuming $l_0 = 0.11$ pc) with the typical observed semidiameter of ammonia cores, ~ 0.05 pc. The statistics of the shapes of actual ammonia cores is not well known; the theoretical model here produces a modest axial ratio in $z{:}\varpi$ of $\sim 2{:}3$ at the density contour $\rho = 30$; at a later time $t = 0.23$ (see below), it becomes 1:2.

The upper left and right diagrams of Figure 4 show the logarithmic density profiles along the ϖ and z-axis for $t = 0$ and $t = 0.21$, respectively. Both profiles in the ϖ and z-directions exhibit a power-law behavior in the range $-0.6 \lesssim \log(\varpi, z) \lesssim 0.0$. (The center is not resolved, and boundary conditions influence the results at large distances from the center.) In an intermediate range, the slope s of the power law, $\rho \propto l^{-s}$, where l corresponds to ϖ or z, is $s \approx 1.0$ for $t = 0$, and $s \approx 1.8$ for $t = 0.21$. The latter exponent is close to the value 2 that characterizes a singular isothermal sphere (*dashed line*), where the dimensional density $\rho = (a^2/2\pi G)r^{-2}$. (See Shu 1977.)

The mass-to-flux distribution $dM/d\Phi$ (for a flux tube which crosses the equator at the radius ϖ) and the integrated mass $M(\Phi)$ interior to a given flux tube Φ as a fraction of the total $M_{\rm tot}$ are shown, for both times, as the lower left and lower right diagrams of Figure 4. Because the magnetic field diffuses relative to the matter, at $t = 0.21$ the quantity $dM/d\Phi$ for the central flux tube has increased by a factor of 1.5 relative to $t = 0$. This modest amount of flux loss can produce the dramatic increase in central concentration seen in this model because of the relative importance of magnetic support compared to thermal support in the initial state. When even a fraction of this support is lost, the gas adjusts, not only by contracting across field lines, but also by sliding down them to

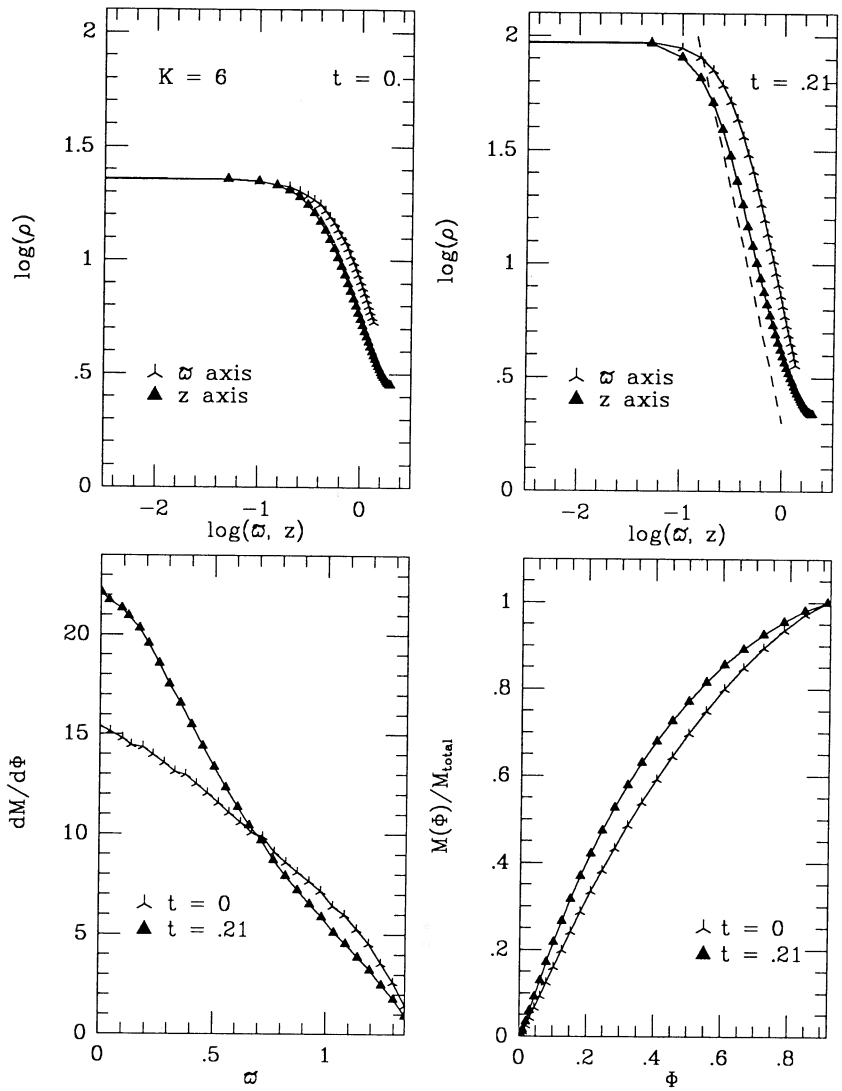

FIG. 4.—Evolution of the case $K = 6$. The logarithmic density profiles along the ϖ- and z- axes $t = 0$ and $t = 0.21$ are given in the upper left and right diagrams, respectively. The dashed line gives the density profile for the singular isothermal sphere, $\rho = (a^2/3\pi G)r^{-2}$ expressed in nondimensional units. The lower left diagram displays, for both times, the mass-to-flux distribution $dM/d\Phi$ for a flux tube which crosses the equator at ϖ; the lower right diagram, the mass $M(\Phi)$ enclosed within flux tube Φ as a fraction of the total $M_{\rm tot}$ in the tidal lobe.

greatly concentrate the material in the central regions. Thus, ambipolar diffusion can play a crucial part in bringing pieces of molecular clouds much closer to conditions of (local) gravitational collapse without having (yet) had a large role in the resolution of the overall magnetic flux problem. This fact goes a long way to settling the ongoing controversy between Mouschovias (1987) and Nakano (1988) concerning when clouds suffer dynamical collapse and magnetic fields decouple (see also SAL). Logically and mechanically, these issues involve two separate topics; tying them together with the name *dynamical decoupling* serves only to confuse the argument. In our models, dynamical collapse is initiated while the field is still reasonably well coupled to the bulk of the gas; the major episode of flux loss (decoupling) must occur at much higher central densities when self-gravitation has already overwhelmed the magnetic and thermal means of support.

Up to $t = 0.21$, the velocities along field lines are subsonic. Across field lines the neutral velocities are not only submagnetosonic but also subsonic. The velocities increase as the core evolves. As was also found by Nakano (1982) for a different parameter regime, the evolution in the last stages proceeds very rapidly. Figure 5 shows the isodensity contours and magnetic flux tubes, the logarithmic density profiles in the ϖ- and z-directions, the mass-to-flux distribution, and the magnetic field versus density along the equator $z = 0$ at the slightly later time $t = 0.23$. At $t = 0.23$, the mass inside the density contour $\rho = 30$ has increased to 1.6, and the central density has risen to 370, with a power-law exponent for the density distribution at intermediate scales of $s \approx 2$. Along the z-axis, the coefficient in the dimensional relation $\rho = Cr^{-2}$ is well represented by the thermal value $C = a^2/2\pi G$; on the ϖ-axis, C is larger because of the contribution of the magnetic support. Nevertheless, $dM/d\Phi$ for the central flux tubes have not increased very much compared to the time $t = 0.21$. Past $t = 0.23$, the available means of support (mostly thermal and magnetic in the densest parts of the cloud) are unable to prevent a runaway increase of the central density.

We cannot follow the evolution during the stage when the

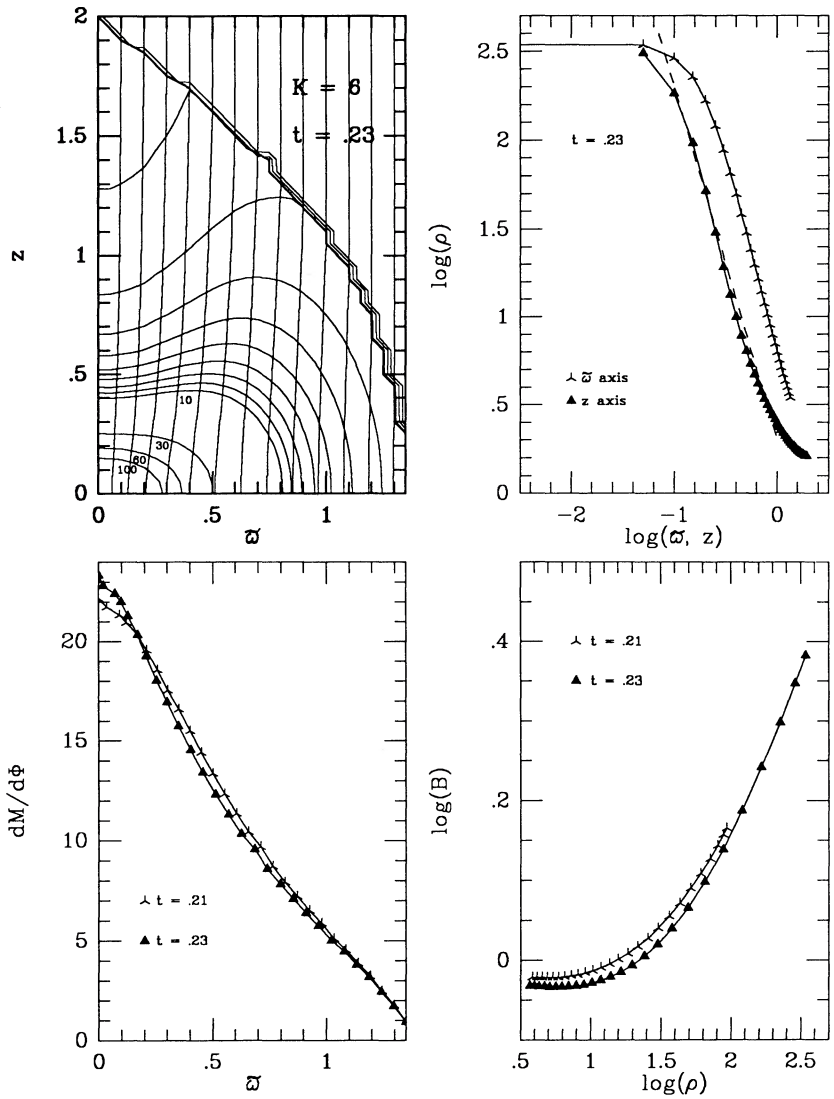

FIG. 5.—Isodensity contours and magnetic flux lines at the time $t = 0.23$ are shown in the upper diagram; logarithmic density profiles along the ϖ- and z-axes, in the upper left diagram. The density contours below $\rho = 10$ are 9, 8, 7, 6, 5, 4, 3, and 2. The dashed line gives the density profile for the singular isothermal sphere, $\rho = (a^2/2\pi G)r^{-2}$ expressed in nondimensional units. The mass-to-flux distribution (*lower left*) and the magnetic field at $z = 0$ vs. density (*lower right*) are displayed for the times $t = 0.21$ and $t = 0.23$.

core tries to develop a central cusp (akin to a singular isothermal sphere) because the flow velocities along field lines (as computed *a posteriori* via the method outlined in the Appendix) approach supersonic values, and the quasi-static assumption breaks down. The increasing density contrast also strains the dynamical-range capabilities of our finite-difference code. Nevertheless, the existing results do suggest that an inside-out collapse initiated from a power-law density distribution is a good description of the dynamical stages of the evolution of (low-mass) protostars (see the review of SAL).

If t_0 equals its "standard" value of 6.0×10^6 yr, this model evolves in $t \sim 1.3 \times 10^6$ yr from an "initial" state with no ammonia emission to a configuration that looks, in its innermost parts, like a classical ammonia core (Fig. 3). After this point, the evolution in the center of the ammonia core proceeds very quickly, reaching a stage of dynamical collapse in another $\sim 10^5$ yr. Such short time scales imply that by the time ammonia cores are observed, an appreciable fraction of the cores should have formed stars. This is in qualitative agreement with the observation (see § I*a*) that roughly half of the ammonia cores show embedded infrared sources (Beichman *et al.* 1986) and with the simple statistical arguments employed by Myers *et al.* (1987). A change in the value of the (somewhat uncertain) fractional ionization coefficient, $\mathscr{C}$, would linearly affect the scaling for the basic time scale t_0, without changing any other part of our calculation (except for the numerical estimates for flow and drift speeds).

b) Evolution with Turbulent Parameter K = 10

The case $K = 10$ corresponds to a turbulent speed that is 58% of the isothermal sound speed at the density $\rho = 30$. Figure 6 shows a superposition of isodensity contours and magnetic flux lines at the time $t = 1.4$ (*solid lines*). The dashed lines indicate the location of the flux tubes at $t = 0$. By outward drift of the ions and field, the core has condensed from an initial central density $\rho_c = 16$ to $\rho_c = 103$. The mass inside the

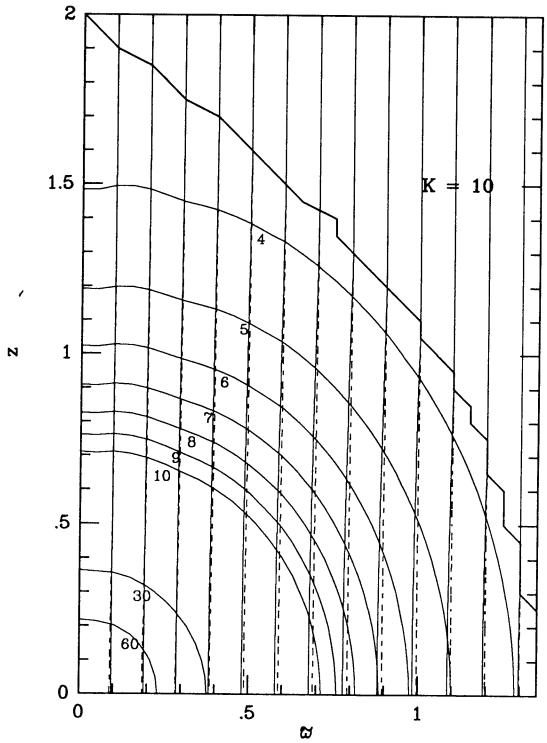

FIG. 6.—The superposition of isodensity contours and magnetic flux tubes for the case with $K = 10$ at the time $t = 1.4$ (*solid lines*). The dashed lines give the magnetic flux tubes at $t = 0$. Compare the density contours here with those at $t = 0$ as shown in Fig. 2.

density contour $\rho = 30$ is 0.86; inside $\rho = 10$, it is 2.45. The axial ratio of the $\rho = 30$ contour is nearly 1:1. From this figure we see that, unlike the case $K = 6$, the magnetic flux tubes have not yet been much dragged in at the center, relative to their position at $t = 0$.

The upper left and right diagrams of Figure 7 show the logarithmic density profiles along the ϖ- and z-axes for $t = 0$ and $t = 1.4$, respectively. The density contrast along the z-axis has increased from 4.4 at $t = 0$, to 35 at $t = 1.4$. The slope of the density power law in the range $-0.6 \lesssim \log(\varpi, z) \lesssim 0.0$ is $s \approx 1.0$ for $t = 0$ and $s \approx 1.6$ for $t = 1.4$. The mass-to-flux distribution $dM/d\Phi$ and the fractional mass M enclosed within flux Φ as a fraction of the total are shown, for both times, as the lower left and lower right diagrams of Figure 7.

We conclude that this model evolves toward a state that looks like an ammonia core in a time scale $\sim 10^7$ yr. This should be contrasted with the model where $K = 6$ for which the corresponding time scale is $\sim 10^6$ yr. The present model takes longer to condense because the drift speed, driven by the Lorentz force $(1/4\pi)(\nabla \times \boldsymbol{B}) \times \boldsymbol{B}$ (see eq. [5]), is smaller in a cloud for which turbulence provides a greater fraction of the total support against self-gravitation.

c) *Evolution with Turbulent Parameter K = 12*

The trend noted above leads to a threshold phenomenon beyond which ammonia cores will not form. The case $K = 12$ corresponds to a turbulent speed that is 63% of the isothermal sound speed at the density $\rho = 30$. Figure 8 shows a superposition of isodensity contours and magnetic flux lines at the time $t = 1.2$ (*solid lines*). The dashed lines indicate the location of the flux tubes at $t = 0$. The core condensed from an initial central density $\rho_c = 14$ only to $\rho_c = 20$, not enough to excite ammonia emission. We stopped the evolution at this time because the mass distribution has remained virtually unchanged since $t = 0.3$, when the magnetic field straightened almost completely by drifting outward relative to the Eulerian grid at all positions in the cloud. Although the magnetic field plays no direct part in cloud support past this point, in a more realistic treatment of interstellar turbulence, even field lines that are straight and uniform *on the average* may have a crucial role as the carrier of momentum transport by Alfvén waves.

The upper left and right diagrams of Figure 9 show the logarithmic density profiles along the ϖ- and z-axes for $t = 0$ and $t = 1.2$, respectively. In the range $-0.6 \lesssim \log(\varpi, z) \lesssim 0.0$, the slope s of the density power law is $s \approx 0.9$ for $t = 0$ and $s \approx 1.0$ for $t = 1.2$. The outer parts of the final configuration has the exponent, but not the coefficient, of a singular logatropic sphere (*dashed line*), which corresponds to an equation of state $P = \mathscr{K} \ln(\rho/\rho_0)$ and a density distribution $\rho = (\mathscr{K}/2\pi G)^{1/2} r^{-1}$. (See Adams, Lizano, and Shu 1988.) This region thus satisfies the empirical relationship for sufficiently large parts of molecular clouds (away from cloud cores) that the column density remains roughly constant independent of size (see, e.g., Solomon *et al.* 1987). The mass-to-flux distribution $dM/d\Phi$ and the mass $M(\Phi)$ contained within flux Φ are shown, for both times, as the lower left and lower right diagrams of Figure 9.

The case $K = 12$ has failed to form an identifiable ammonia core because a stable equilibrium state is accessible to it where the (mean) magnetic field can evolve asymptotically to become straight and uniform, with the total support against self-gravitation taken up by the turbulent and thermal pressure. The evolution from the "initial" state is very slow (characteristic of envelope values) because the drift velocity is proportional to the magnetic stress, and the latter is almost zero. The same conclusion holds with greater force for all models with higher values of the turbulent parameter K. It is reasonable to ask, of course, how a high level of turbulent support in molecular clouds can be physically sustained without the formation of cores and stars (with energetic outflows), but this is a complicated topic whose discussion we defer to § VII.

d) *Summary of Results*

Table 1 shows a summary of results that we obtained with $\mathscr{R} = 7.2$, $2l = 4.0$, and $M_{\rm tot} = 7.0$, with different values of the turbulent parameter K. The entries contain (1) the elapsed time since the "initial" state before the formation of a recognizable dense ammonia core; (2) the masses within the fiducial densities $\rho = 60$, $\rho = 30$, and $\rho = 10$; (3) the average strength of the magnetic field inside the $\rho = 30$ contour.

TABLE 1

SUMMARY OF RESULTS

K	τ[a]	M_{60}[b]	M_{30}[b]	M_{10}[b]	$\bar{B}_{30}$[c]
6.....	0.21	0.26	1.00	2.84	1.29
8.....	0.46	0.53	1.15	2.75	1.18
10.....	1.40	0.31	0.86	2.45	1.10

[a] The time scale τ for the formation of an ammonia core is given in units of t_0.

[b] M_{60}, M_{30}, and M_{10} are, respectively, the mass, in units of m_0, inside the density contour $\rho = 60$, $\rho = 30$, and $\rho = 10$.

[c] $\bar{B}_{30}$ is the average magnetic field, in units of B_0, inside the density contour $\rho = 30$. (For values of the scalings t_0, m_0, and B_0; see § II.)

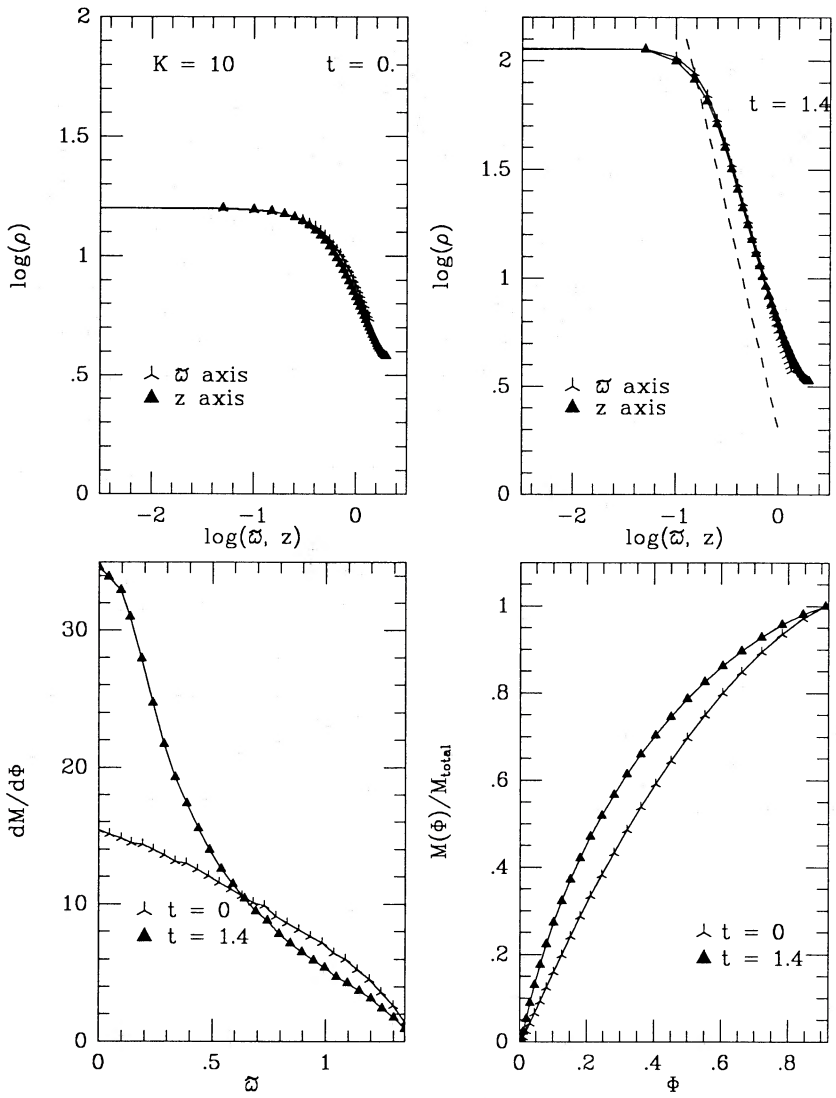

FIG. 7.—Evolution of the case $K = 10$. The logarithmic density profiles along the ϖ- and z-axes $t = 0$ and $t = 1.4$ are given in the upper left and right diagrams, respectively. The dashed line gives the density profile for the singular isothermal sphere, $\rho = (a^2/2\pi G)r^{-2}$ expressed in nondimensional units. The lower left diagram displays, for both times, the mass-to-flux distribution $dM/d\Phi$ for a flux tube that crosses the equator at ϖ; the lower right diagram, the mass $M(\Phi)$ enclosed within flux tube Φ as a fraction of the total M_{tot} in the tidal lobe.

The average magnetic fields inside the density contour $\rho = 30$ are larger for models with smaller K because the magnetic field shares a greater fraction of the burden for support against self-gravity. Figure 10 shows that the magnetic field on the equator at $t = 0$ is proportional to ρ^{κ} where $\kappa \sim 0.2$–0.4, in qualitative agreement with the behavior found by other authors for self-gravitating clouds with similar (relatively flat) mass-to-flux distributions (e.g., Mouschovias 1976). However, only limited density contrasts and magnetic field variations are attainable for stable configurations having such relatively flat mass-to-flux distributions, in conflict with observations of real molecular clouds. Fortunately, when the turbulent parameter K is less than a threshold value ($K \approx 11$), the density at the center can increase with time due to the occurrence of ambipolar diffusion. The accompanying increase of magnetic field demonstrates that, at the characteristic densities associated with cloud cores, good frictional coupling still exists between neutrals and ions (and magnetic field). Notice that a power-law scaling $B \propto \rho^{\kappa}$ holds only in the innermost regions. In the outer regions, B actually drops below the envelope value (because no flux has been allowed to cross the tidal lobe) through the inward movement of interior field lines. (Since magnetic fields are frozen to the ions, relative motion between ions and neutrals can act, in general, to increase the field strength at one place in the cloud only at the expense of decreasing it elsewhere.) Figure 11 shows that the magnetic field in the center tends to increase with density as a function of time roughly as ρ_c^{κ} where $\kappa \sim 0.5$ (see, e.g., Scott and Black 1980), but only in circumstances when the gravitational contraction along and across field lines more than makes up for the losses due to ambipolar diffusion (case $K = 6$ and the later stages of $K = 10$ as compared to $K = 12$; see also Nakano 1984). All in all, then, Figures 10 and 11 should provide strong caution against the indiscriminate use of scaling relationships of the type $B \propto \rho^{\kappa}$ to interpret observational data, since the nonunique coefficient of proportionality depends sensitively on the evolutionary history of the self-gravitating region.

Finally, we note that the tubulence in these models is always

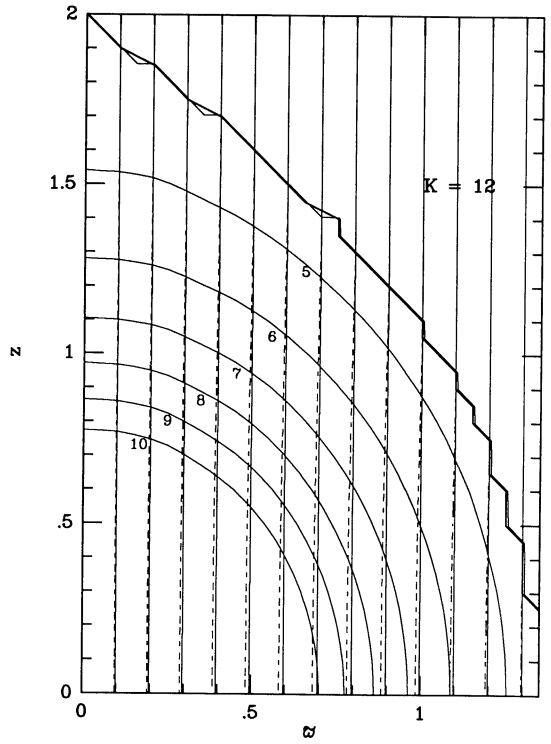

FIG. 8.—The superposition of isodensity contours and magnetic flux tubes for the case $K = 12$ at the time $t = 1.2$ (*solid lines*). The dashed lines give the magnetic flux tubes at $t = 0$. Compare the density contours here with those at $t = 0$ as shown in Fig. 2.

sub-Alfvénic. The ratio of the turbulent and Alfvén speeds at any point is

$$\frac{v_{\rm turb}}{v_{\rm A}} = \frac{K^{1/2}}{\mathscr{R}B} .$$

With $\mathscr{R} = 7.2$ and $B \gtrsim 1$, this ratio is always less than unity for the models presented here; indeed, it is everywhere less than 0.48 for $K = 12$ and less than 0.34 for $K = 6$. For real molecular clouds, some sort of self-regulating mechanism involving nonlinear waves may be at work to keep the density dependence of $v_{\rm turb}$ the same as $v_{\rm A}$ (thereby "explaining" eq. [10]) when B does not have large spatial variations (see the discussion in SAL).

VI. CRITICAL AND UMBRAL MASSES

The name "critical mass" has traditionally been reserved for the mass that can be supported against self-gravity by the global magnetic field (e.g., Mestel 1965; Mouschovias and Spitzer 1976; Mestel and Ray 1985; but see TIN). If thermal pressure is the only other agent of support, this nomenclature causes little confusion for large molecular clouds where magnetic fields play a much more important role. However, turbulence can modify conditions in the envelope of a cloud (which contains the bulk of the mass) by factors of order 2, so we propose to modify the standard convention by using the name "magnetic critical mass" for the expression in equation (1), and by defining another kind of critical mass via the virial theorem. For a static distribution of gas, well coupled to magnetic fields, the scalar virial theorem, in dimensional units, reads (see the trace of eq. [22] on p. 580 of Chandrasekhar 1961):

$$\int \left(3P + \frac{B^2}{8\pi} - \rho \boldsymbol{x}\cdot\nabla V\right) d^3x = \int \left[\frac{1}{8\pi}(|\boldsymbol{B}|^2\boldsymbol{x} - 2\boldsymbol{x}\cdot\boldsymbol{BB}) + P\boldsymbol{x}\right]\cdot \boldsymbol{n}\, d^2x ,$$

where the right-hand side involves an integral over a surface (with outward unit normal $\boldsymbol{n}$) that encloses the volume involved in the integration on the left-hand side. If we schematically perform the integrations over the tidal lobe, we can write the resulting expression as

$$2\alpha a^2 M + \beta^2(2\pi\mathscr{K})L^3 + \gamma^2 B_0^2 L^3 - GM^2/L = 0 , \quad (33)$$

where we have normalized the coefficient of the self-gravitational term and absorbed the effects of the surface terms and the details of the volume integration into the dimensionless coefficients α, β, and γ (not to be confused with the drag coefficient γ in eqs. [5], [15], and [39]). In particular, a straightforward application of the divergence theorem demonstrates that the surface and volume terms cancel identically for a constant pressure P or magnetic field $\boldsymbol{B}$.

If we apply the virial theorem to the critical state and regard it as a quadratic equation for the critical mass, we may solve equation (33) to obtain

$$M_{\rm cr} = M_a + (M_a^2 + M_K^2 + M_B^2)^{1/2} . \quad (34)$$

In the above, M_a is the thermal mass

$$M_a \equiv \alpha(a^2/G)L \quad (35)$$

and equals $\alpha/2$ times the mass inside a radius L of a singular isothermal sphere; M_K is the turbulent mass

$$M_K \equiv \beta(2\pi\mathscr{K}/G)^{1/2}L^2 \quad (36)$$

and equals β times the mass inside the radius L of a singular logatropic sphere; and M_B is the magnetic critical mass

$$M_B \equiv \gamma(B_0/G^{1/2})L^2 , \quad (37)$$

with $\gamma = 1.4c$ if we wish to bring our configurations in accord with equation (1).

Without referring to the fiducial envelope density ρ_0, note that M_a, M_K, and M_B are the only three masses one can obtain with the dimensional parameters of the problem: the gravitational constant G, the sound speed a, the turbulent parameter $\mathscr{K}$, the magnetic field B_0, and the separation between the cells $2L$. Given the actual total (dimensional) mass $M_{\rm tot}$ inside the tidal lobe, we can form only three independent nondimensional mass ratios: $M_a/M_{\rm tot}$, $M_K/M_{\rm tot}$, and $M_B/M_{\rm tot}$. For the models in § V, these three dimensionless ratios are related to l, K, and $\mathscr{R}$ through $M_a/m_0 = \alpha l$, $M_K/m_0 = \beta(K/2)^{1/2}l^2$, and $M_B/m_0 = \gamma\mathscr{R}l^2$, with $M_{\rm tot}/m_0 = 7.0$. Our experience (see below) leads us to advocate the values, $\alpha = 1.1$ and $\beta = 0.47$, for centrally condensed states that are marginally stable to gravitational collapse.

All of the models presented in this paper have masses $M_{\rm tot}$ less than the critical mass defined by equation (34); by our new definition, they correspond to *subcritical* states. Initially subcritical states that are magnetically supercritical, $M_{\rm tot} > M_B$, could, in principle, be induced to collapse gravitationally without any loss of magnetic flux (conservation of $M_B \propto B_0 L^2$) by a large external compression (e.g., decrease of L) that suffi-

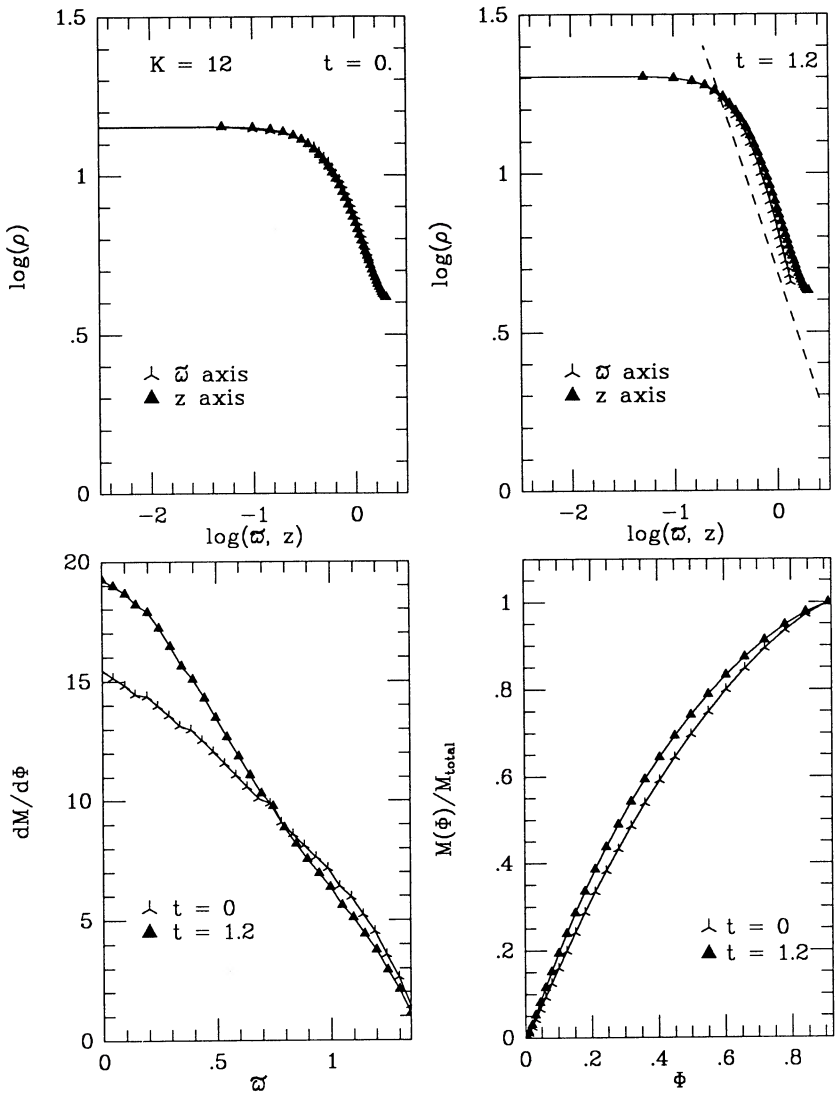

FIG. 9.—Evolution of the case $K = 12$. The logarithmic density profiles along the ϖ- and z-axes $t = 0$ and $t = 1.2$ are given in the upper left and right diagrams, respectively. The dashed line gives the density profile for the singular logatropic sphere, $\rho = (\mathscr{K}/2\pi G)^{1/2} r^{-1}$, expressed in nondimensional units. The lower left diagram displays, at both times, the mass-to-flux distribution $dM/d\Phi$ for a flux tube that crosses the equator at ϖ; the lower right diagram, the mass $M(\Phi)$ enclosed within flux tube Φ as a fraction of the total $M_{\rm tot}$ in the tidal lobe.

ciently lowers M_a and M_K to make the final state supercritical. In the absence of such effects, secular evolution of subcritical states can be achieved only by flux redistribution, in which case the evolutionary outcome bifurcates into two distinct regimes. Ambipolar diffusion acts so as to try to straighten out the magnetic field lines and make them uniform. If the cloud can succeed in doing this, the magnetic forces ultimately vanish, and the cancelling of the surface and volume terms in the virial theorem gives $\gamma = 0$ in the expression (37) for M_B. When $M_B = 0$ in the final state, we call the resulting expression for equation (34), the *umbral* mass (pronounced ŭmbrál, the Spanish word for threshold):

$$M_{\rm um} = M_a + (M_a^2 + M_K^2)^{1/2} . \qquad (38)$$

If the mass $M_{\rm tot}$ (inside the tidal lobe) exceeds $M_{\rm um}$ (e.g., the case $K = 6$ in the previous section), we say the region is *superumbral*, and ambipolar diffusion will sooner or later cause the formation of a dense core that becomes increasingly dark (invoking the sense of the latin root "umbra"). In the superumbral case, the self-gravitation is strong enough to continue to pull in the field lines, despite the ongoing ambipolar diffusion. If, on the other hand, the mass $M_{\rm tot}$ is less than $M_{\rm um}$ (e.g., the case $K = 12$ in the previous section), we say the region is *subumbral*, and ambipolar diffusion can straighten out the field lines without the production of an ever denser central region that eventually leads to the birth of a star.

By constructing a closely spaced evolutionary sequence of models for $M_{\rm tot}/m_0 = 7.0$, $2l = 4.0$, $\mathscr{R} = 7.2$, we determined $K = 11$ to correspond to the *umbral* case. We subsequently built a set of equilibria (like our initial states) with $M_{\rm tot}/m_0 = 7.0$, $2l = 4.0$, $\mathscr{R} = 4.5$, and artificially lowered K until force-balance iterations no longer converged. In this manner, we found that $K = 4.0$ corresponds to the *critical* case for the new set of parameters. From equations (38) and (34), with $\gamma = 0.19$ in the latter, we obtain two constraints for the coefficients α and β. Solving these constraints yields the values $\alpha = 1.1$ and

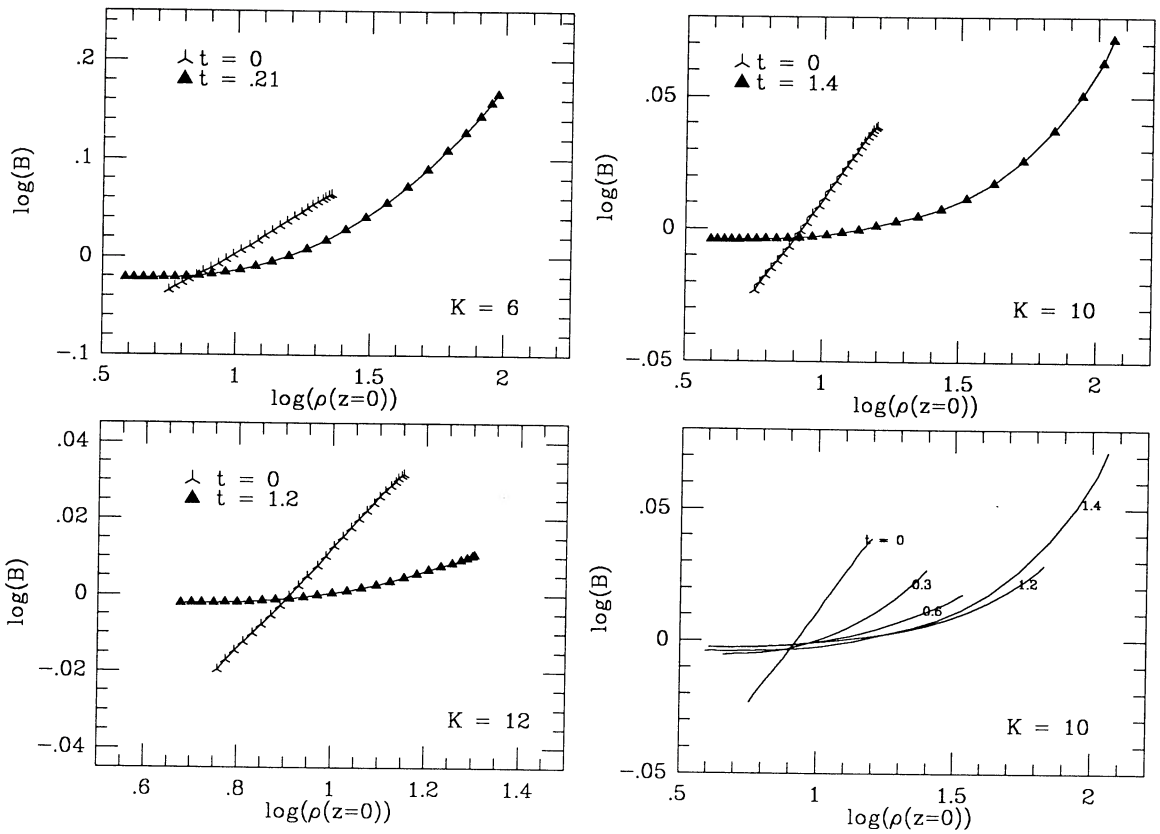

FIG. 10.—Relationships between log (B) and log (ρ) in the equatorial plane. In the case $K = 6$ (*upper left*), ambipolar diffusion has failed to prevent the magnetic field from being dragged in by the neutrals as the core condenses gravitationally. In the case $K = 10$ (*upper and lower right*), the magnetic field succeeds is drifting out (even relative to an Eulerian description) for times earlier than $t = 1.2$, but the strong gravity eventually wins and begins to drag the field in along with the condensing core. In the case $K = 12$ (*lower right corner*), the magnetic field monotonically drifts from the inside to the outside, and by the time $t = 1.2$, ambipolar diffusion has nearly established a uniform (and straight) field configuration.

$\beta = 0.47$ mentioned earlier. (It is possible to derive the same conclusions by performing the virial integrations directly.) The formulae (34)–(38) now permit us to extend the overall results of our study to portions of parameter space not directly covered by our model survey. In particular, notice that if the turbulence is negligible, equation (38) gives $M_{\rm um} = 2M_a$, nearly equal to the mass of the singular isothermal sphere (because $\alpha \approx 1$) inside a radius L.

Figure 12 shows a plot of the ratio of umbral mass to critical mass, $M_{\rm um}/M_{\rm cr}$, versus the ratio of the mass inside the tidal lobe to the critical mass, $M_{\rm tot}/M_{\rm cr}$, for the set of models with dimensionless spacing $2l = 4.0$ and magnetic parameter $\mathscr{R} = 7.2$, when the turbulent parameter varies from $K = 0$ (*leftmost solid triangle*) to $K = 11$ (*umbral case*) to $K = 30$ (*rightmost open triangle*). There are three regions in the plane: supercritical ($M_{\rm tot} > M_{\rm cr}$), subcritical-superumbral ($M_{\rm um} < M_{\rm tot} < M_{\rm cr}$) and subcritical-subumbral ($M_{\rm tot} < M_{\rm um} < M_{\rm cr}$). In the first case, the cloud as a whole collapses dynamically, fragments, and forms either a bound cluster or a tight group of OB stars (see § I). In the second case, dense ammonia cores are formed by ambipolar diffusion; these cores will collapse from inside-out and form (predominantly low-mass) stars. In the third case, unless the turbulence decays, no runaway core collapse or star formation will occur.

When cores do form with central densities that exceed either $\rho_{\mathscr{K}} \equiv \mathscr{K}/a^2 \equiv K\rho_0$, or $\rho_B \equiv B_0^2/4\pi a^2 \equiv \mathscr{R}^2\rho_0$ ($\gg \rho_0$ if magnetic fields dominate over thermal pressure in supporting the envelope), they tend to acquire power-law profiles, $\rho \approx Cr^{-2}$, where r is the dimensional distance from the center of the core, with an effective C somewhat greater than the value $a^2/2\pi G$ appropriate for a singular isothermal sphere (or "equivalent sound speed" $a_{\rm eff}$ somewhat greater than a; see Stahler, Shu, and Taam 1980, and SAL). If we assume slip speeds v_d to approach sonic values, the formation of a central cusp and attendant core runaway can be estimated to occur with a characteristic time scale t_* (cf. eq. [5] with lengths that scale as at_* and densities that scale as $1/4\pi Gt_*^2$):

$$t_* = \left[\frac{\gamma\mathscr{C}}{(4\pi G)^{1/2}}\right]^{1/2}\left(\frac{a}{G^{1/2}B_0}\right), \qquad (39)$$

$\sim 3 \times 10^5$ yr using "standard" molecular cloud parameters.[2]

VII. CONCLUSIONS

a) *Limitations of the Present Study*

In this paper we have studied the origin of dense cores by the process of ambipolar diffusion in molecular clouds. To obtain a tractable problem, we have made a number of simplifying assumptions—quasi-static evolution, axial symmetry, fixed tidal lobe, and so on—the most serious of which are the following.

[2] Notice that the quantity in the second bracket of equation (39) equals the time scale $(4\pi G\rho_B)^{-1/2}$. For "standard" parameters, notice also the numerical coincidence between ρ_B and the critical density needed to excite ammonia emission.

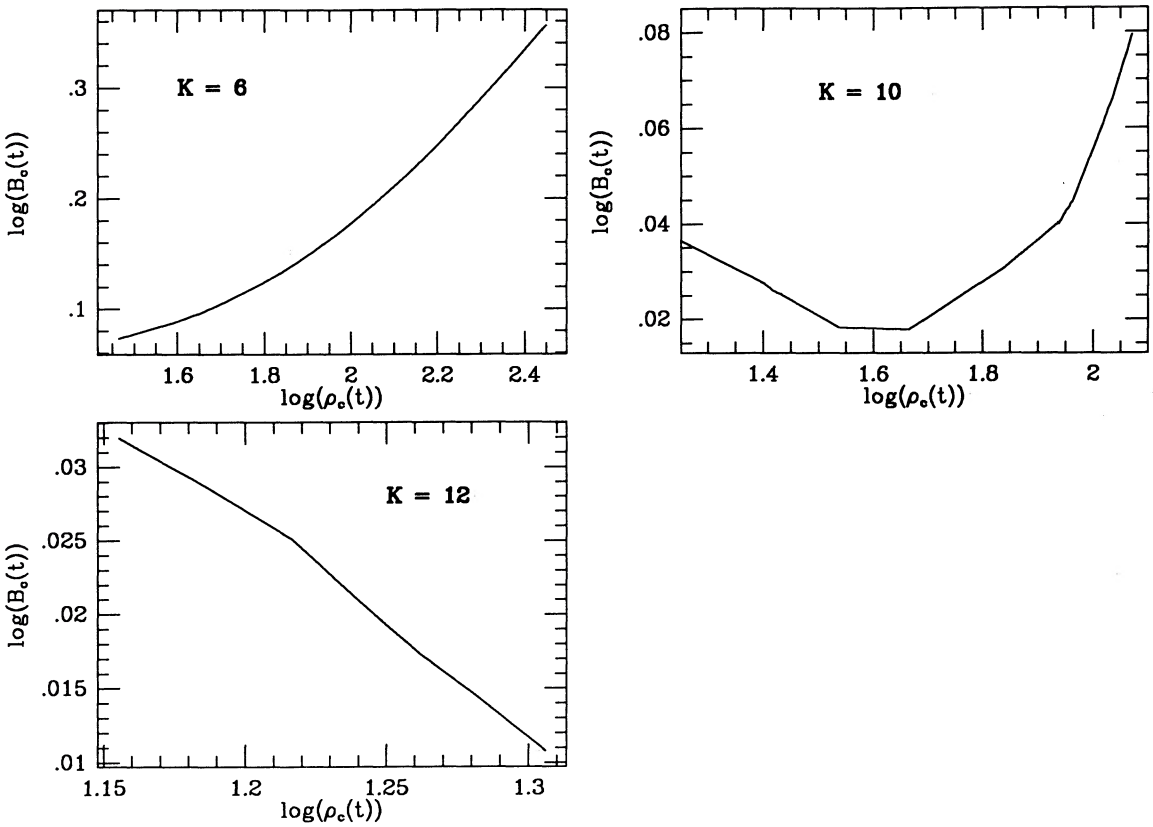

FIG. 11.—Evolution of the central values of the magnetic field and gas density. The quantities log (B_c) and log (ρ_c) are plotted for the different cases, demonstrating that the formation of an ammonia core ($K = 6$ and $K = 10$) is accompanied (eventually) by an increase of B_c, while failure to produce a dense core ($K = 12$) results in the gradual straightening of the magnetic field lines.

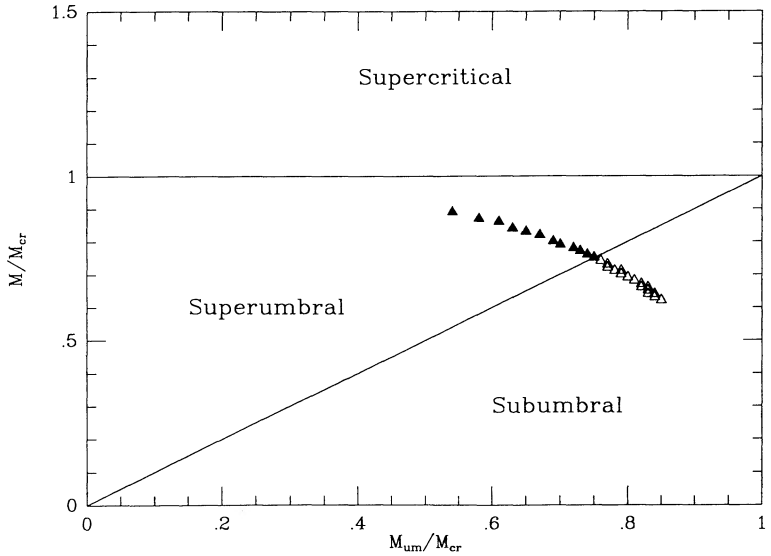

FIG. 12.—The ratio of umbral mass to critical mass, M_{um}/M_{cr}, vs. the ratio of the total mass in the tidal lobe to the critical mass, M_{tot}/M_{cr}. The symbols refer to the set of models with dimensionless spacing $2l = 4.0$ and magnetic parameter $\mathcal{R} = 7.2$, with the turbulent parameter varying from $K = 0$ (*leftmost solid triangle*) to $K = 11$ (*umbral case*) to $K = 30$ (*rightmost open triangle*). In the supercritical case, $M_{tot} > M_{cr}$, the cloud as a whole collapses and possibly fragments; in the subcritical-superumbral case, $M_{um} < M_{tot} < M_{cr}$, dense ammonia cores form by ambipolar diffusion and collapse from inside-out to form stars; in the subcritical-subumbral case, $M_{tot} < M_{um} < M_{cr}$, unless the turbulence decays, no core or star formation will occur.

1. Cloud turbulence, which probably represents an ensemble of nonlinear Alfvén waves (Arons and Max 1975; Zweibel and Josafatsson 1984; Myers 1987; Shu 1987), has been mimicked in an ad hoc manner as a scalar pressure, satisfying the simple barotropic equation of state $P_{\rm turb} = \mathscr{K} \ln(\rho/\rho_0)$. Unlike the isothermal sound speed a, for which we do possess a good theoretical understanding (see, e.g., de Jong, Boland, and Dalgarno 1980 or Lizano and Shu 1987), our treatment of turbulent motions—in particular, the value of the constant $\mathscr{K}$ (whose nondimensional analog is K)—currently rests entirely on a semi-empirical foundation.

2. We do not have an *a priori* explanation (from considerations of the global structure of the cloud clump, for example) for the mean separations $2L$ of cloud cores. In our calculations, we merely rely on observations to give us the value for $2L$ (or its nondimensional analog $2l$).

3. The calculations of Moushovias (1976) and TIN do provide some theoretical guidance to estimate the strength B_0 of the magnetic field in the common envelope of a molecular cloud. However, construction of such models depends on a specification of the mass-to-flux distribution, which requires a theory of molecular cloud formation. In the absence of a definitive theory, we need to call upon observations (see, e.g., Goodman *et al.* 1988) for knowledge concerning B_0 (or its nondimensional analog $\mathscr{R}$).

4. We have ignored the motions of individual cores in a larger cloud clump with respect to one another; we have also ignored the dynamical effects of rotation; and by adopting the assumption of force balance at the outset, we have forfeited the ability to follow the transition to the fully dynamical stages of contraction.

Of these limitations, a simple extension of the existing calculations could help to include the main effects of rotation. Until the cloud goes into dynamical collapse, magnetic fields tend to enforce uniform rotation at an angular rate Ω parallel to the mean field (Gillis, Mestel, and Paris 1979; Mouschovias and Paleologou 1980; Strom *et al.* 1985; Heyer 1986). Such a state of affairs could easily be accounted for by the introduction of an effective potential $V_{\rm eff} = V - \Omega^2 \varpi^2/2$. In contrast, the development of powerful multidimensional magnetohydrodynamic codes may be necessary to make fundamental theoretical progress on some of the other problems. In particular, the elucidation of the global structure and evolution of large molecular clouds (both of the supercritical and subcritical variety) constitutes one of the dominant challenges for future developments.

b) *Accomplishments of the Present Study*

Within the objectives of the present study, where we regard l^2K, $l\mathscr{R}$, and $M_{\rm tot}/l$ (see footnote 1) as adjustable free parameters (to be obtained from observations), we have derived several useful results. In particular, we have learned that:

1. The process of ambipolar diffusion can naturally explain the sizes, densities, and time scales for the production of dense cores of the type first surveyed by Myers and Benson (1983) in the Taurus dark cloud. For quiescent regions (in terms of turbulent support), the time required to produce regions characterized by appreciable ammonia emission is 10^6 yr or less; for more active regions, it can exceed 10^7 yr.

2. Unless the turbulence decays, ammonia cores will not form in very active regions, where the total mass $M_{\rm tot}$ inside the tidal lobe is less than a threshold value $M_{\rm um}$ defined by equation (38). The existence of such a threshold implies that the molecular clouds may have many "failed" cores in regions where the turbulence has been increased, say, by the winds from neighboring low-mass protostars. Such a picture might even form a physical basis for current suggestions concerning the role of "self-regulation" in star formation (e.g., Norman and Silk 1980; Franco 1984).

3. Dense ammonia cores will only be produced in superumbral regions, where $M_{\rm tot} > M_{\rm um}$. During the last stages of the evolution of such objects, a core runaway develops on a characteristic time scale of a few times 10^5 yr, in which the density profile steepens into a power-law form, $\rho \propto r^{-s}$, with s approximately equal to 2. In the models, the magnetic field inside the ammonia core increases relatively little with respect to the background, not because there is a large amount of ambipolar diffusion, but because a bit, together with gas settling along field lines, goes a long way toward producing a central density cusp and the beginning of an inside-out core collapse. In agreement with the results of Nakano (1988) and Nakano and Umebayashi (1986*a*, *b*), we find that the onset of dynamical collapse (when the neutral velocities approach sonic values) occurs typically before the mass-to-flux ratio for the central flux tube has been enhanced by more than a factor of 2 from the initial state. The resolution of the magnetic flux problem for forming stars must therefore occur at densities much higher than we normally associate with ammonia cores.

4. Molecular-line radio astronomers have found numerous instances of large flattened structures surrounding newly formed stars, having a scale of $\sim$0.01–0.1 pc (e.g., Kaifu *et al.* 1984; Sargent *et al.* 1988; Rudolph 1988). Unless the structures can be shown to be centrifugally supported, we would warn against their interpretation in terms of disks. In many (perhaps most) cases, they may be the remnants of the magnetically supported cores calculated in this paper (for example, after a bipolar outflow has blown away the polar caps; see Mathieu *et al.* 1988). Magnetic support by itself naturally produces flattened configurations, although the flattening is typically not very severe for the regime of parameter space relevant to Taurus molecular cloud cores. Rotation parallel to the magnetic field would produce additional flattening in the cores, but, observationally, rotation is not dynamically important at the stage of the ammonia cores (Myers, Goodman, and Benson 1989). Core shapes, then—especially at the lower density-contour levels—are generally not good indicators of physical conditions (thereby causing perhaps some of the ambiguity in Heyer's 1986 results) because they are too easily influenced by extraneous factors (such as tidal forces).

5. The size and mass of a cloud core depend on the molecule with which it is observed, since different molecules trace different critical densities. In this paper we have concentrated on the masses and sizes of the cores as observed with the NH_3 molecule. Fuller (1988) has observed these cores in an optically thin transition of $C^{18}O$, which traces less dense material ($\sim 2 \times 10^3$ cm^{-3}). In a preliminary analysis, he obtains sizes that are a few and masses that are several times larger than obtained by the ammonia measurements, in qualitative and semiquantitative agreement with the predictions of the models in this paper.

6. The above comments (see also § V*a*) support the view that the reservoir of material potentially available in subcritical clouds to form stars is much greater than the mass that actually ends up in the completed objects. We believe that it is a stellar wind which reverses the infall of matter onto the protostar and ultimately defines its mass (see the review of SAL).

Considerations of the physics of the interstellar medium, such as those given in the present paper, do not automatically produce, *by themselves*, mass scales characteristic of the fundamental objects of astronomy, the luminous stars.

This work has been funded in part by grant No. AST86-14743 from the National Science Foundation and in part under the auspices of a special NASA astrophysics theory program which supports a joint Center for Star Formation at NASA Ames Research Center, UC Berkeley, and UC Santa Cruz. In addition, S. L. thanks the National University of Mexico for continued fellowship support during her tenure as a Berkeley graduate student.

APPENDIX

ESTIMATE OF NEUTRAL VELOCITIES

Because of the quasi-static assumption, there is no direct information about the vector velocity of the neutrals $\boldsymbol{u}_n$. Nonetheless, it is possible to estimate it in the following way.

a) Velocity Perpendicular to the Flux Tube

Let s be the length coordinate measured along the flux tube from the midplane $z = 0$. The drift velocity $\boldsymbol{v}_d = \boldsymbol{u}_i - \boldsymbol{u}_n$ at a point s of a flux line labeled by Φ is parallel to $\nabla\Phi$, i.e., perpendicular to the flux tubes. Because the magnetic field is tied to the ions, $\partial\Phi/\partial t + \boldsymbol{u}_i \cdot \nabla\Phi = 0$, the velocity of the ions in the direction perpendicular to the flux tubes is given by

$$u_{i\perp} = -\frac{\partial\Phi/\partial t}{|\nabla\Phi|} \tag{A1}$$

The quantity $\nabla\Phi$ is known, and we obtain $\partial\Phi/\partial t$ in the first part of the operator splitting of D/Dt discussed in § III. The component of the neutral velocity perpendicular to the flux tubes, $u_{n\perp}$, at the point s can now be calculated as

$$u_{n\perp} = u_{i\perp} - v_d \,. \tag{A2}$$

b) Velocity Parallel to the Flux Tube

In the second part of the operator splitting, the neutrals try to "settle" along field lines to achieve hydrostatic equilibrium. A complication enters because vector force balance prevents the flux tubes from remaining fixed on an Eulerian grid after a diffusion time step, but this (perpendicular) motion does not affect the velocity component parallel to flux tubes. The total rate of change of the mass m between two flux tubes labeled Φ and $\Phi + d\Phi$ and lying between the equatorial plane $z = 0$ and the point s has two contributions,

$$\left(\frac{\partial m}{\partial t}\right)_d + \left(\frac{\partial m}{dt}\right)_s , \tag{A3}$$

where $(\partial m/\partial t)_d$ is due to ambipolar diffusion and $\partial m/\partial t)_s$ is due to the settling along flux tubes.

The first part of the operator split (the diffusion step) yields $(\partial m/\partial t)_d$, which is of no interest to us here. Dividing the change in m at a given s resulting from the second part of the operator split (force balance with flux freezing) by the elapsed time (between net combined steps) yields $(\partial m/\partial t)_s$. Kinematically, however, this quantity also equals

$$\left(\frac{\partial m}{\partial t}\right)_s = -\int u_{n\|}(s)\rho \frac{2\pi\varpi\, d\Phi}{(\partial\Phi/\partial\varpi)_s} = -u_{n\|}(s)\int \frac{\partial^2 m}{\partial s\,\partial\Phi}\, d\Phi = -u_{n\|}(s)\left(\frac{\partial m}{\partial s}\right)_t , \tag{A4}$$

where the minus sign indicates that a negative parallel velocity of the neutrals $u_{n\|}$ increases the mass m in the flux tube below the position s. From equation (A4), we deduce the reasonable result that the velocity parallel to the flux tube Φ at a point s is simply the Lagrangian velocity associated with the settling to come into force balance:

$$u_{n\|} = (\partial s/\partial t)_m \,. \tag{A5}$$

Equation (A5) provides a simple prescription to compute the parallel component of the neutral velocity.

REFERENCES

Adams, F. C., Lada, C. J., and Shu, F. H. 1987, *Ap. J.*, **312**, 788.
Adams, F. C., and Shu, F. H. 1986, *Ap. J.*, **308**, 836.
Arons, J., and Max, C. E. 1975, *Ap. J. (Letters)*, **196**, L77.
Benson, P. J. 1983, Ph.D. thesis, Harvard University.
Beichman, C. A., Myers, P. C., Emerson, J. P., Harris, S., Mathieu, R. D., Benson, P. J., and Jennings, R. E. 1986, *Ap. J.*, **307**, 337.
Chandrasekhar, S. 1939, *An Introduction to Stellar Structure* (Chicago: University of Chicago Press).
———. 1961, *Hydrodynamic and Hydromagnetic Stability* (Chicago: University of Chicago Press).
Dame, T. M., Elmegreen, B. G., Cohen, R. S., and Thaddeus, P. 1986, *Ap. J.*, **305**, 892.
de Jong, T., Dalgarno, A., and Boland, W. 1980, *Astr. Ap.*, **91**, 68.
Draine, B. T., Roberge, W. G., and Dalgarno, A. 1983, *Ap. J.*, **264**, 485.
Elmegreen, B. G. 1979, *Ap. J.*, **232**, 729.
Franco, J. 1984, *Astr. Ap.*, **137**, 85.
Fuller, G. A. 1988, Ph.D. thesis, University of California, Berkeley.
Fuller, G. A., and Myers, P. C. 1987, in *NATO/ASI Physical Processes in Interstellar Clouds*, ed. M. Scholer (Dordrecht: Reidel), p. 137.
Gillis, J., Mestel, L., and Paris, R. B. 1979, *M.N.R.A.S.*, **187**, 311.
Goodman, A. A., Crutcher, R. C., Heiles, C. H., Myers, P. C., and Troland, T. H. 1989, in preparation.
Heyer, M. H. 1986, Ph.D. thesis, University of Massachusetts.
Kaifu, N., Suzuki, S., Hasegawa, T., Morimoto, M., Inatani, J. 1984, *Astr. Ap.*, **134**, 7.
Keto, E. R., Ho, P. T. P., and Haschick, A. D. 1987, *Ap. J.*, **318**, 712.

Lada, C. J., and Wilking, B. A. 1984, *Ap. J.*, **287**, 610.
Larson, R. B. 1981, *M.N.R.A.S.*, **194**, 809.
Lizano, S. 1988, Ph.D. thesis, University of California, Berkeley.
Lizano, S., and Shu, F. H. 1987, in *NATO/ASI Physical Processes in Interstellar Clouds*, ed. M. Scholer (Dordrecht: Reidel), p. 173.
Mathieu, R. D., Benson, P. J., Fuller, G. A., Myers, P. C., and Schild, R. E. 1988, *Ap. J.*, **330**, 385.
McKee, C. F. 1989, *Ap. J.*, submitted.
Mestel, L. 1965, *Quart. J.R.A.S.*, **6**, 265.
———. 1985, in *Protostars and Planets II*, ed. D. C. Black and M. S. Matthews (Tucson: University of Arizona Press), p. 320.
Mestel, L., and Ray, T. P. 1985, *M.N.R.A.S.*, **212**, 275.
Mestel, L., and Spitzer, L. 1956, *M.N.R.A.S.*, **116**, 503.
Moneti, A., Pipher, J. L., Helfer, H. L., McMillan, R. S., and Perry, M. L. 1984, *Ap. J.*, **282**, 508.
Mouschovias, T. Ch. 1976, *Ap. J.*, **206**, 753.
———. 1978, in *Protostars and Planets*, ed. T. Gehrels (Tucson: University of Arizona Press), p. 209.
———. 1987, in *NATO/ASI Physical Processes in Interstellar Clouds*, ed. M. Scholer (Dordrecht: Reidel), p. 491.
Mouschovias, T. Ch., and Paleologou, E. V. 1980, *Ap. J.*, **237**, 877.
———. 1981, *Ap. J.*, **246**, 48.
Mouschovias, T. Ch., Paleologou, E. V., and Fiedler, R. A. 1985, *Ap. J.*, **291**, 772.
Mouschovias, T. Ch., and Spitzer, L. 1976, *Ap. J.*, **210**, 326.
Myers, P. C. 1987, in *Interstellar Processes*, ed. D. Hollenbach and H. Thronson (Dordrecht: Reidel), p. 71.
Myers, P. C., and Benson, P. J. 1983, *Ap. J.*, **266**, 309.
Myers, P. C., Fuller, G. A., Mathieu, R. D., Beichman, C. A., Benson, P. J., Schild, R. E., and Emerson, J. P. 1987, **319**, 340.
Myers, P. C., and Goodman, A. 1988, *Ap. J.*, **329**, 392.
Myers, P. C., Goodman, A., and Benson, P. J. 1989, in preparation.
Nakano, T. 1979, *Pub. Astr. Soc. Japan*, **31**, 697.
———. 1982, *Pub. Astr. Soc. Japan*, **34**, 337.
———. 1983, *Pub. Astr. Soc. Japan*, **35**, 209.
———. 1984, *Fund. Cosmic Phys.*, **9**, 139.
Nakano, T. 1985, *Pub. Astr. Soc. Japan*, **37**, 69.
———. 1988, in *Galactic and Extragalactic Star Formation*, ed. R. Pudritz and M. Fich (Dordrecht: Reidel), in press.
Nakano, T., and Umebayashi, T. 1986*a*, *M.N.R.A.S.*, **218**, 613.
———. 1986*b*, *M.N.R.A.S.*, **221**, 319.
Norman, C., and Silk, J. 1980, *Ap. J.*, **238**, 158.
Rudolph, A. 1988, Ph.D. thesis, University of Chicago.
Sargent, A. I., Beckwith, S., Keene, J., and Masson, C. 1988, preprint.
Scott, E. H. 1984, *Ap. J.*, **278**, 396.
Scott, E. H., and Black, D. C. 1980, *Ap. J.*, **239**, 166.
Scoville, N. Z., Yun, M. S., Clemens, D. P., Sanders, D. B., and Waller, W. H. 1987, *Ap. J. Suppl.*, **63**, 821.
Shu, F. H. 1977, *Ap. J.*, **214**, 488.
———. 1983, *Ap. J.*, **273**, 202.
———. 1987, in *Star Formation in Galaxies*, ed. C. Persson (NASA CP. 2466), p. 743.
Shu, F. H., Adams, F. C., and Lizano, S. 1987, in *Ann. Rev. Astr. Ap.*, **25**, 23 (SAL).
Solomon, P. M., Rivolo, A. R., Barret, J. W., and Yahil, A. 1987, *Ap. J.*, **319**, 730.
Solomon, P. M., and Sanders, D. B. 1985, in *Protostars and Planets II*, ed. D. C. Black and M. S. Matthews (Tucson: University of Arizona Press), p. 59.
Stahler, S. W., Shu, F. H., and Taam, R. E. 1980, *Ap. J.*, **241**, 637.
Strittmatter, P. A. 1966, *M.N.R.A.S.*, **132**, 359.
Strom, S. 1988, in *Galactic and Extragalactic Star Formation*, ed. R. Pudritz and M. Fich (Dordrecht: Reidel), in press.
Strom, S. E., Strom, K. M., Grasdalen, G. L., Sellgren, K., and Wolff, S. 1985, *A.J.*, **90**, 2281.
Tomisaka, K., Ikeuchi, S., and Nakamura, T. 1988, *Ap. J.*, **326**, 208 (TIN).
Vrba, F. J., Strom, K. M., and Strom, S. E. 1976, *A.J.*, **81**, 958.
Welch, Wm. J., Dreher, J. W., Jackson, J. M., Terebey, S., and Vogel, S. N. 1987, *Science*, **238**, 1550.
Wilking, B. A., and Lada, C. J. 1983, *Ap. J.*, **274**, 698.
Zweibel, E. G. 1988, *Ap. J.*, **329**, 384.
Zweibel, E. G., and Josafatsson, K. 1983, *Ap. J.*, **270**, 511.

SUSANA LIZANO: Instituto de Astronomía, Apdo. 70-264, UNAM, 04510 México D. F., México

FRANK H. SHU: Astronomy Department, University of California, Berkeley, CA 94720